Designing and testing a prototype stable-wing-support system to deploy, retrieve, and operate a horizontal river hydrokinetic turbine within the water column to achieve cost-effective power generation in cold climates

by

Ibrahim Aqdiam

A Thesis Submitted to the Faculty of Graduate Studies of

The University of Manitoba

In partial fulfillment of the requirements of the degree of

MASTER OF SCIENCE

Department of Mechanical Engineering

The University of Manitoba

Winnipeg

Abstract

River hydrokinetic turbines harness renewable energy in river currents to contribute to microgrids. Despite many hydrokinetic turbine designs, systems still require reducing costs and operate effectively in cold climates. A stable-wing-support system is developed and tested to deploy, retrieve, and operate within the water column of a horizontal axis river turbine. The prototype design addresses identified stability problems using a fixed-wing design previously tested in a laboratory water tunnel and an energetic river. The stable-wing-support system prototype uses a NACA 0012 airfoil with 6°, 10°, and 15° dihedral angles designed using open-source Xflr5 software to optimize the lift, drag, and moment coefficients for angles of attack from -5° to +15°. The prototype also includes a winged tail to improve the turbine assembly's stability further. The stable-wing-support prototype designed using SolidWorks is 3-D printed. Tests are conducted to quantify the stability of the stable-wing-support prototype using a water tunnel at flow velocities varying from 0.5 to 1 m/s, resulting in Reynold's numbers from 3.37×10^5 to 6.74×10^5. Stability data is recorded and analyzed using open-source Tracker software and then exported to MATLAB software for analysis. Results indicate that the stability of the stable-wing-support system with dihedral angles 6°, 10°, and 15° and a winged tail significantly improves the stability by 80%, 50%, and 40%, respectively, compared to a previous design for flow velocities up to 1 m/s, addressing the objectives of this research and contribute a design to maximizing power production in cold climates.

Acknowledgment

I would like to express my deepest gratitude to all those who have supported and contributed to this research project. I am grateful to my advisor, Dr. Eric Bibeau, for his invaluable guidance, insightful feedback, and unwavering support throughout the research process. His expertise and encouragement have been instrumental in the completion of this work. I would also like to extend my heartfelt thanks to my technician, Zeev Kapitanker, and my colleagues, Abbas Dharamsi, Laetitia Duret, Malcolm Paintin, and Ishan Tandon, whose constructive discussions and collaborative spirit in all steps have greatly enriched this project. My sincere appreciation goes to the funding bodies, Mitacs and Dragon, for their financial support, which made this research possible. I am also indebted to my family for their constant encouragement and understanding during the challenging times of this research journey. Their patience and support were a source of strength for me. Last, I would like to acknowledge the contributions of all the participants and institutions involved in this study. Without their cooperation and input, this research would not have been possible. Thank you all for your invaluable support and contributions.

Contents

List of Tables

List of Figures

Abbreviations

AOA	Angle of attack
BEMT	Blade element momentum theory
BSM	Bottom structure mounting
CFD	Computational fluid dynamics
CHTTC	Canadian Hydrokinetic Turbine Testing Centre
FSM	Floating structure mounting
GW	Gigawatt
HKTs	Hydrokinetic turbines
HP	Hydropower
kW	Kilowatt
LCOE	Levelized cost of energy
MW	Megawatt
MRE	Marine renewable energy
NSM	Near-surface structure mounting
RHKTs	River hydrokinetic turbines
SWS	Stable-wings-support
VFD	Variable frequency drive

Nomenclature

A	Area
Ar	Anchor rope
Cd	drag coefficient
ch	Chord length
Cl	Lift coefficient
Cm	Moment coefficient
D	Drag force
H	Height
H_w	Water depth
L	Lift force
Le	Length
M	Pitching moment
Ma	Anchor mass block
θ	Pitch angle
ρ	Fluid density
P	Power
q	Dynamic pressure
Re	Reynolds number
S	wingspan
T	Temperature
μ	Dynamic viscosity
V	Flow velocity

y	Depth

1 Introduction

1.1 The transition to renewable energy

Highly carbon-based centralized power systems can be replaced in part with renewable micro-grid systems [1]. For example, Canada has approximately 300 diesel communities that burn diesel fuel to meet their power needs, which are not linked to a centralized grid [2], [3]. These diesel communities have started installing solar photovoltaics. Powering such remote communities affordably and dependably is a challenge, even when community renewables rank high in terms of priorities [4], [5], [6]. Community efforts on how they use their renewable energy resources can differ significantly [7], [8]. Such communities are exposed to increasing levels of energy insecurity [1] but are learning how renewable energy can reshape their power infrastructure [9], [10] and are implementing renewable energy initiatives [11], [12]. The conversion of their power systems from diesel to renewables can improve their economic performance [8], [9]. Such communities look at opportunities to improve their independence and energy sovereignty [1], [13]. This approach requires that energy investments are aligned with the skills, values, knowledge, and capabilities of these communities [14]. Thus, implementing renewable energy is becoming part of the community planning process [15], [16]. Holdmann et al. [8] conclude that renewable energy systems can better support remote communities [17]. Given the importance of transitioning to renewable energy for remote communities, much work remains to develop commercial-ready renewable energy technologies for remote applications. Adaptation of renewable technologies to remote communities has received insufficient attention [18], [19], [20], [21].

1.2 River hydrokinetic turbines

Hydropower plants use a dam or reservoir to form a head, which is then used by conventional hydro turbines to produce power [22]. Hydropower plants have some disadvantages, such as massive civil work and flooding of lands in catchment areas [23], [24], [25], [26], [27]. However, the best hydropower plant locations have been mostly taken [28], [29]. Alternatively, river hydrokinetic turbine (RHKT) systems convert the kinetic energy in a flowing water stream to mechanical power, albeit at a much smaller scale [30], [31], [32].

A RHKT operate under the same physics as a wind turbine. RHKT can be classified depending on whether the rotating axis is aligned with the flow (horizontal axis turbines) or normal to the flow (vertical and cross-flow turbines) [33], [34]. The turbines are generally located at the surface or the bottom of a river, as shown in Figure 1. The energy at the river bottom is much less due to the boundary layer by approximately 30% to 60% [35]. They can also be potentially located within the water column.

The economics of RHKT remain challenging to ascertain as costs depend on the application location, and RHKT is not yet a mature technology. The power output of a hydrokinetic turbine is directly proportional to the flow velocity cube, and the estimate speculates that higher velocities can reduce costs [36], [37]. Thus, RHKT systems present a promising alternative to traditional hydropower plants by harnessing the kinetic energy of flowing water without the need for extensive civil infrastructure. However, the economic viability of RHKT remains a challenge due to the high levelized cost of energy (LCOE) and the nascent stage of the technology [37]. Figure 2 shows how typical RHKT systems are deployed.

Figure 1: The Canadian Hydrokinetic Turbine Test Centre (CHTTC) evaluates different types of RHKT. The left image shows a near-surface RHKT positioned to maximize exposure to the free stream velocity. The right image depicts a bottom-mounted RHKT featuring a mounting structure that elevates the rotor above the boundary layer for optimal performance.

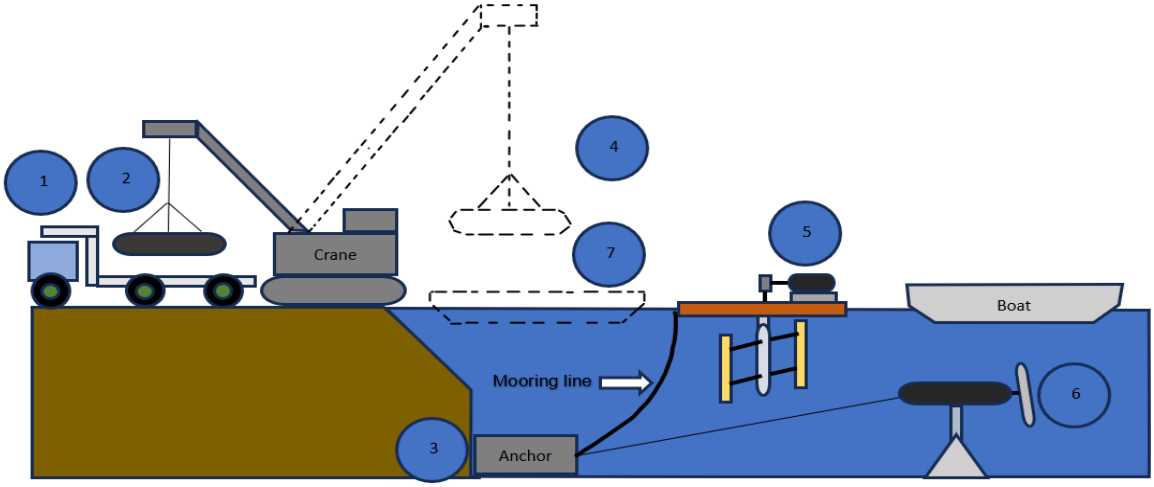

Figure 2: This illustration outlines the procedures for operating an RHKT in riverine environments: (1) transporting the turbine to the designated site, (2) setting up the RHKT, (3) establishing an anchor point, (4) deploying the RHKT using a launch ramp or crane, and (5) securing the RHKT to the anchor for operation. Bottom-mounted turbines are advantageous for year-round use but may incur higher costs due to complex deployment and retrieval processes. Surface turbines can be retrieved using a boat, while pontoons are typically used for bottom-mounted RHKT. For clarity, the turbine and anchor are shown rotated by 90 degrees. Additional details are provided in Table 1.

1.3 Cold climate issues with RHKT

Cold climates significantly impact RHKT systems in several ways. One of the primary challenges is the formation of frazil ice that can obstruct water surface-mounted RHKT systems, reduce the output power, and thus adversely affect RHKT. This ice formation is particularly concerning in northern regions, leading to significant energy losses [38]. Additionally, ice poses substantial risks, as it can encase equipment and potentially cause catastrophic damage to RHKT, especially during the spring break-up of ice sheets. This is particularly problematic in remote or off-grid communities [38]. Many strategies have been tested to reduce the effect of ice on surface-mounted RHKT systems, such as ice booms and forebays with ice covers. However, the impact of cold climates on RHKT systems is significant and expensive. In addition, safety concerns in cold conditions may also restrict water surface-mounted RHKT systems operations [43]. It has been shown that RHKT must be placed below the water surface in cold weather applications to survive.

Bottom-mounted RHKT solves the ice issue, but deployment requires skilled personnel and many vessels over multiple days. These systems also operate at lower velocities due to boundary layer effects affecting power output. The higher turbine deployment and retrieval costs increase the LCOE for bottom-mounted RHKT [39], [40] and have additional implications for safety and training. These factors highlight the need for a better design for RHKT in cold climates to mitigate ice impacts and ensure efficient power generation.

Operating turbines within the water column is an option and solves both issues of ice and slow velocity, but it is more complex, and there is insufficient data to support or reject this design approach for cold climate applications. Thus, there is a critical need to study turbines that operate

within the water column. Our research team focuses on developing a stable-wing-system (SWS) to operate RHKT within the water column. As such, there are presently no turbine designs that operate within the water column that can produce in the energetic region of the flow and overcome ice issues. The proposed SWS offers a potential solution to these challenges by simplifying deployment and retrieval processes and enabling operation below the ice in the water column, thereby maximizing power output. The SWS could significantly reduce costs and enhance the market acceptance of RHKT systems in cold climates. By addressing the stability and operational challenges associated with RHKT, the SWS approach could play a crucial role in advancing the commercial readiness of hydrokinetic energy technologies, ultimately contributing to a more sustainable and diversified energy portfolio. By simplifying and reducing the costs of deployment and retrieval and operating efficiently below the ice in the water column, the SWS could maximize power generation in cold climates [41]. The SWS could represent a significant step in making renewable energy technologies commercially viable for remote applications.

1.4 SWS

Our research group hypothesizes that the SWS in cold climates can address the high LCOE for RHKT and provide better performance in winter by

- simplifying and reducing costs of deployment and retrieval,
- operate below the ice in the water column to maximize power,
- making components contribute to deployment, retrieval, and operations,
- allow switching the rotor easily by a small crew to match seasonal velocities better and significantly increase the yearly power factor and
- eliminating the need for a shroud by using a low RMP generator without a gearbox reduces weight and allows for a rotor change.

The SWS is a support structure that allows the installation, retrieval, and operation of the horizontal turbine within the water column without a shroud. The objective is to utilize components for multiple purposes to reduce costs. SWS may help overcome the high LCOE and allow it to reach market acceptance in cold climates. This hypothesis is presently restricted to relatively small-scale systems. The SWS approaches our team developed are depicted in Figure 3, and employs:

1. Ballast in the nacelle and wings to facilitate the turbine's deployment, retrieval, and operation within the water column.
2. Wing and tail design adds the required static and dynamic stability.
3. The water current is used to fly the RHKT using the SWS. The SWS's positive angle of attack (AOA) generates a lift force that allows the system to fly, and a negative AOA submerses the turbine in the water column.
4. the aerodynamic centre, centre of mass, and centre of buoyancy coincide for simplicity.
5. A three-point wire harness is required to fly the turbine and change its AOA using a drogue line. The length ratios of the three wires control the final location of the turbine in the water column, a function of the river velocity.
6. A lever arm is located on the top front of the SWS. Its function is to change AOA by pulling backward or pushing forward a lever arm activated by an above drogue line, resulting in surfacing or submerging the turbine within the water column. This is accomplished by changing the harness wire lengths.
7. A buoy is positioned on the water surface which marks the location of the mooring line to connect the turbine and is used to connect a drogue line to surface or sink the RHKT from a boat by shorting one of the 3 harness ropes detailed later.

8. A two-blade rotor significantly simplifies deployment and retrieval by having the RHKT require a low water clearance.

Figure 3 illustrates the steps for deploying a SWS for RHKT. The process starts by placing the turbine in the water and configuring the system for transportation. A vessel moves the turbine to the anchor buoy. To achieve this configuration, the SWS is horizontally oriented and floated during transit. The system is then connected to the mooring line connected to the anchor. The anchor holds the SWS by absorbing the drag exerted through the mooring line. The primary components of the system are (1) a marine power cable, (2) two wings with dihedral angles to fly the RHKT and improve its stability, (3) a tail to further improve the stability, (4) a lever arm to adjust the AOA for surfacing and submerging the turbine, and finally (5) a horizontal turbine. Once the mooring and electrical lines are fastened to the SWS, the system is submerged by activating the lever. The wings are positioned optimally in the water column at a positive AOA to allow the SWS to fly carrying the RHKT in the water column, and the drogue line connects to a buoy on the water surface to activate retrieval. The flow velocity, combined with the positive AOA of the SWS, generates a lift force to fly the RHKT in the water column. A 3-point harness is configured ahead to adjust the final turbine depth.

During operation, the turbulence caused by the flow velocity will generate instability for the RHKT; the SWS has a dihedral angle and a tail, which allows the system to maintain its flight. The SWS is designed to improve the roll and yaw stability so that the SWS returns to its original position when turbulence, boils, and large eddies affect the system. The SWS allows the RHKT to operate within the water column and not impede boat traffic, elements carried by flooding, and ice

formation on the water surface and the bottom of the river. The SWS is designed to make it simple to deploy and retrieve an RHKT operating below the water surface. This also allows for a change in the rotor size to produce more power in winter months, as shown by Bahador [42].

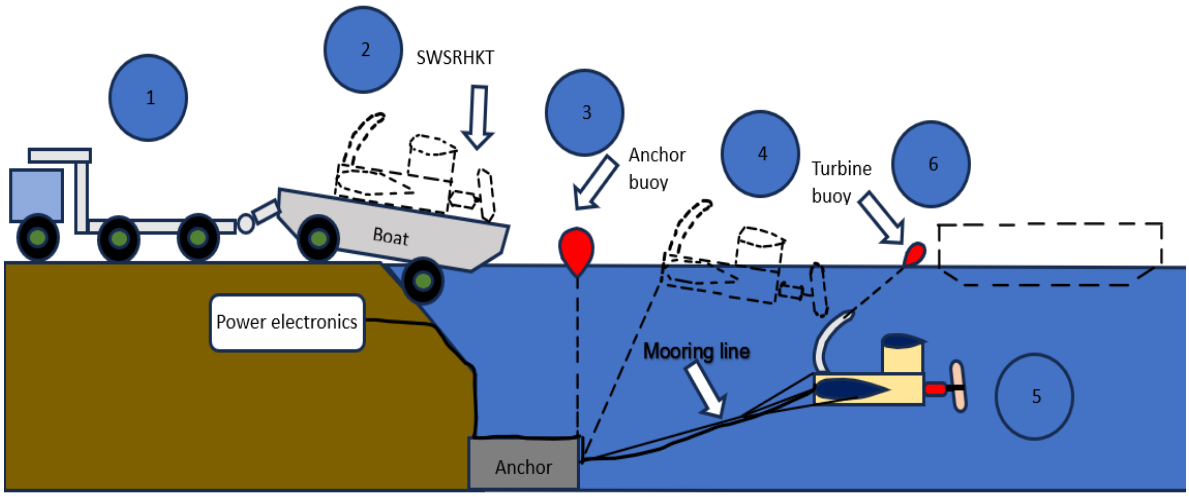

Figure 3: The SWS reduces the need for on-site personnel and costly procedures. The development process includes (1) transporting the turbine to the site, (2) assembling the SWS, (3) positioning the anchor point in the river and attaching an anchor buoy to secure the mooring line, (4) using a pontoon or on-shore winch to float the SWS to the designated location, where the RHKT will be deployed with the SWS on the water surface; and (5) & (6) attaching a small buoy to the lever arm and pushing it forward to create a negative AOA, allowing the SWS to submerge into the water column. For clarity, the turbine is shown rotated 90 degrees in-plane. Additional details are provided in Table 1.

Table 1 summarizes the primary stages of the conventional RHKT life cycle, as opposed to the proposed SWS approach.

Table 1: A comparison between SWS and the current RHKT processes with labels associated with Figures 2 and 3 (table over 2 pages)

No.	Operation	Current RHKT technique	Proposed SWS technique
1	Delivery	The transportation of turbines necessitates the utilization of sizable trailers or specialized shipping containers to accommodate their support structure.	The turbine is transported on a pontoon boat, which minimizes shipping requirements because no support structure is needed. Additionally, the generator is integrated into the SWS.
2	Setup	Installing the turbine at the site location usually requires powerful tools, lifting cranes, and electrical equipment before it can be put into operation.	No assembly is necessary for the riverine turbine; it is vital to do pre-diagnostic tests.
3	Preparation on site	Both surface and bottom-mounted turbines can utilize anchors positioned on the river bottom. An anchor buoy is attached to the mooring line to guarantee that there is always a single accessible place on the river's surface.	A bottom-mounted anchor bears the entire drag load on the mooring line. It secures the turbine and acts as an intermediary point for the main line, which carries the power and instrumentation between the turbine and the shore.
4	Deployment	Large RHKT systems often require a crane or a sizable lifting loader. Boats are commonly used for small-scale surface deployments, while pontoons are utilized for more giant turbines installed on the bottom.	The turbine installation necessitates a designated launch site and potentially a delivery vessel, contingent upon the distance separating the launch site and the selected anchor points.
5	Operation and maintenance (in summer)	The operation of surface-mounted turbines presents minor challenges and allows for easy maintenance due to the accessibility to the surface. Bottom-mounted turbines require a costly retrieval and redeployment technique to be maintained.	The turbine operates like a bottom-mounted turbine but can be accessible from the water surface. It can be retrieved by pulling the lever arm, which is connected to a small buoy, backward. This action allows for a larger AOA, driving the SWS to the surface.
6	Operation and maintenance (in winter)	According to Bibeau et al. in [43] and [44], surface-mounted turbines are generally unable to operate during winter due to the accumulation of ice at the interface between the water and air. However, bottom-mounted turbines can still function because they are fully submerged underwater. Nevertheless,	While in operation, the turbine is fully immersed in the water column, enabling it to prevent the formation of ice and avoid the accumulation of ice and debris. If feasible, maintenance should be postponed until the spring season.

		maintaining these turbines in cold climate conditions can be challenging.	
7	Retrieval	Surface-mounted retrieval is accomplished by moving the RHKT from the mooring line connection to shore or employing a winch from shore to pull the turbine. Pontoon vessels are commonly used to support bottom-mounted turbines, as they can endure the significant drag forces exerted by the river and provide ample space for transporting the turbines.	The retrieval procedure entails prepping the SWS for transportation by altering the AOA to expose the turbine's surface. An alternative method to move the floating SWS to shore is to use a boat or employ an additional rope to connect the SWS to land and pull the turbine to shore.

1.5 Objectives

1- Design an SWS to deploy, operate, and retrieve an RHKT and determine the optimal dihedral angle and design to enhance system stability.

2- Build a scaled SWS prototype and test it in a water tunnel to evaluate the stability of the system.

2 Literature review

This section reviews aspects of RHKT advancements as they relate to the deployment, operation, and retrieval of turbines which includes:

- Overview of marine energy
- Motivation to commercialize river hydrokinetic turbines
- Operation principles
- Resource assessment
- Need for RHKT
- Types of RHKT
- Commercially available turbines
- Riverine turbine challenges
- Problems with the adoption of RHKT
- Impact of cold weather
- Mounting arrangements\
- Riverine turbine economic analysis
- Performance evaluation of riverine turbines

2.1 Overview of marine energy

The rapid growth in global primary energy demand is projected to rise by over 25% by 2040 to approximately 206,000 TWh/year, and increasing electricity needs place significant pressure on renewable energy sources [45]. Marine Renewable Energies (MRE) are expected to play a vital role in meeting these demands, offering utility-scale power generation due to the abundance of ocean-based energy resources. MRE, including wave, tidal, and ocean currents, hold theoretical

potential near 151,300 TWh/year, close to global primary energy consumption in 2017, but many technologies remain in their infancy [46]. Offshore wind is the most mature MRE sector, but wave and tidal technologies face challenges due to high LCOE and environmental factors. The SWS for RHKT offers a strategic approach to overcoming these challenges, particularly in cold climates, where MRE deployment faces added difficulties such as ice cover and harsh conditions. By simplifying the deployment and retrieval processes, the SWS directly addresses one of the significant cost drivers in RHKT operations. Furthermore, its ability to operate below the ice in the water column allows for continuous power generation during winter, maximizing energy capture and improving reliability.

Several studies demonstrate that resource variability, siting, and environmental impacts are critical for optimizing hydrokinetic energy systems. For instance, Fouz et al. [47] Musa et al. found significant seasonal variability in the Minho Estuary, where river discharges enhance energy potential in winter and spring. Musa et al. [48] emphasized that strategic siting of marine hydrokinetic turbines can mitigate sediment transport while maintaining power generation.

Lust et al. [49] explored how surface waves can enhance energy recovery in hydrokinetic turbines through vortex transport, highlighting the importance of integrated design strategies for optimizing power capture. Stratigaki et al. [50] emphasize the need for integrated near and far-field modeling to maximize performance and environmental compatibility. This focus on modularity and optimization mirrors the SWS approach, where each component enhances system efficiency and reduces operational costs. In addition, the SWS is designed to be fully submerged, which inherently reduces the physical disturbance to the water surface and surrounding habitats compared

to surface-mounted systems. This design choice helps mitigate the impact on marine life, particularly in sensitive riverine environments where surface activities can disrupt aquatic ecosystems. The deployment of the SWS aims to minimize habitat disruption by avoiding extensive construction or excavation on the riverbed. This approach is crucial for protecting fish habitats and maintaining the natural flow regime, which is essential for the health of aquatic ecosystems. By reducing the need for invasive installation methods, the SWS aligns with the hypothesis of achieving cost-effective power generation without compromising environmental integrity. The research acknowledges that flow velocity and turbulence can affect marine life, mainly fish and other aquatic organisms. The SWS's design seeks to optimize flow interaction to minimize turbulence and avoid creating hazardous conditions for marine life. This consideration is vital for ensuring that the system operates harmoniously within the natural environment, supporting the hypothesis of sustainable energy generation. The research emphasizes the importance of ongoing monitoring and adaptation to ensure that the SWS does not adversely affect marine life. This includes assessing the system's impact on local species and making necessary adjustments to mitigate adverse effects. Such adaptive management strategies are integral to developing an economically viable and environmentally responsible system.

2.2 Motivation to commercialize RHKT

RHKT systems are being commercially developed partly to support microgrids and climate change [23]. These turbines could be beneficial in terms of LCOE, and local employment and allow an increase in the percentage of renewable energy in communities [51]. These turbines can generate electricity in remote communities with nearby resources [52]. Unlike RHKT, convectional hydro plants remain one of the best options for electrifying rural communities. However, they require large upfront capital and can provide a strong cost-to-reliability trade-off in the long term [53].

The hydro plants provide base power with their capacity factors changing with the seasons but can attract negative attention due to their impact on the riverine environment [53], [54], [55].

An alternative is for small communities to investigate RHKT as part of their clean energy plan. Here, the community first needs to identify the resources nearby and understand what RHKT technology is suitable for deployment locally to provide power year-round, including making sure that cold weather and monsoons, if any, do not destroy installations. Table 2 This section shows some of RHKT's more recent projects. Although this technology is still developing, improvements are required to contribute to a market-acceptable LCOE for communities.

Table 2: Sample of recent RHKT projects installed around the world to extract energy from the flowing water

No.	Project name	Location	Company	Turbine type
1	Chilla Power Channel	India	DLZ Corp	Axial-flow 25-kW
2	Neyveli Lignite	India	Smart Hydropower in collaboration with Imp Powers	Axial-flow 4 x 5-kW array
3	Kakkad HEP	India	Imp Powers using Smart Hydro tribune	Axial-flow 5 x 5-kW array
4	Duncan Dam	Kaslo, British Columbia	Instream Energy Systems	Cross-flow
5	Roza Canal	Yakima, Washington		
6	Tiger Project	France and UK	Hydroquest	Cross-flow
7	Sluice of Cutch icon Afsluitdijk, Wadden Sea	UK	Torcado	Axial flow
8	Pointe du Bois Canadian Hydrokinetic Turbine Testing Centre	Manitoba, Canada Winnipeg River, Manitoba	New Energy	Cross-flow
9	RITE	Canada and USA	Verdant	Axial-flow
10	Seeneoh	River Garonne in Bordeaux, France	Gkinetic	Cross-flow 25-kW

2.3 RHKT and its principle of operation

As the generated power for RHKT is function times velocity cubed, these can be viable at a stream velocity of above 0.5 m/s [56] but preferably above 2 m/s. Although there are other proposals for harnessing river currents, the turbine has become the most implemented approach. Like wind turbines, the power output of the RHKT is dependent on the same parameters such as density, cross-sectional area, turbine power coefficient, and velocity cubed. Water boasts an approximately 800 times higher density value than wind [57]. Thus, the RHKT generates significantly more power than an analog windmill of equal diameter under similar conditions.

One operational principle of RHKT involves the horizontal axis design. In this configuration, the rotor transforms kinetic energy from water flow into mechanical energy. The rotor consists of multiple blades connected to a central hub, and its design is critical for maximizing turbine efficiency. Optimizing power generation requires careful attention to the rotor's geometry. Various factors influence its performance, such as the tip speed ratio, blade count, airfoil shape, power coefficient, solidity, angle of attack (AOA), and chord line [33]. The maximum power of a RHKT available in water is determined by [58]:

$$P = \frac{1}{2} \rho A V^3 \quad (1)$$

where, P is power, ρ is water density, A is the rotor area, and V is flowing velocity.

2.4 Resource assessment

The requirements to establish a hydrokinetic energy-producing site depend on variable velocities and the rivers' water levels during energy extraction [59]. Even though most evaluations of hydrokinetic resources have been done on a small scale, there are currently promising large-scale attempts. Despite global river datasets, they do not fit the data analysis for the river energy, as the fluctuations are considerable. A simulation that modeled the effect of the turbines on the water

level was conducted to discover the actual volatility. The water fluctuation due to the decline in the downstream lake was found to be many times more than estimated. The power coefficient was calculated using the velocity profiles from various measurement locations [23], [60]. Recent studies evaluate how to develop hydrokinetic systems in a river site, meaning the study of the available resources and full-time operation. These studies put the hydrokinetic sites into context by first considering the sites with reasonable potential in the hydrologic, hydraulic, ecological, and economic contexts. After that, they engage in the detailed technical design of a prototype, and a row of turbines.

Ridgill et al. [61] conducted a study using a 35-year reconstructed daily discharge record to estimate the theoretical global riverine hydrokinetic resource (excluding Greenland) at 58,000 TWh/year, equivalent to a mean power of 6.7 TW. The study presented a global spatial distribution by individual river reaches and grouped by country, identifying China, Russia, and Brazil as having the highest overall potential. After normalizing by total river length, Bhutan, Nepal, and Tajikistan also showed significant potential. Evaluating the accuracy of power and energy yield estimates for 2.94 million river reaches is challenging; thus, the results should be viewed as a first-order approximation, including where the most promise lies.

conducted an early study evaluating the technical potential of riverine hydrokinetic resources in the USA. Their research identified the most promising river sections in 12 out of 16 hydraulic regions, chosen based on factors such as average discharge and flow velocities exceeding 1.3 m/s. The assessment assumed turbine arrays covering 25% of the river's width and length, meeting the discharge threshold, with turbine spacing set at half the turbine diameter within rows and five

diameters between rows. The turbine diameter was 80% of the mean depth, and a power coefficient (CP) of 40% was used. This approach estimated a total mean annual power generation of 12,500 MW, producing 110 TWh/year. UMA Group [63] carried out a study in Canada to evaluate the hydrokinetic potential of selected rivers that met minimum criteria: $Q > 450$ m³/s, $V > 1.5$ m/s, width over 50 m, and depth exceeding 3 m. The analysis assumed uniform conditions over extended river stretches and applied the Manning formula. Data was sourced from topographic maps and HYDAT, a database that archives daily and monthly averages of flow, water levels, and sediment concentrations across Canada [64]. More than half of the global population resides within 3 km of a freshwater body, while only 10% live farther than 10 km from one [65]. A strong correlation exists between population density, electrification needs, poverty levels, and the distribution of rivers [66]. Hydrokinetic energy conversion technology is estimated to be 15-20 years behind wind power generation [67]. This study's approach to designing an SWS for RHKT aims to support the development of this technology, addressing the RHKT resource assessment as an essential step.

As a result, resource assessment is a pivotal step in developing hydrokinetic energy sites, as it provides a comprehensive understanding of the potential and challenges associated with harnessing riverine energy. Despite the complexities and fluctuations in river data, recent studies have made significant strides in estimating the global and regional hydrokinetic potential, highlighting promising areas for development. Integrating detailed hydrologic, hydraulic, ecological, and economic analyses into the site selection process ensures that hydrokinetic projects are feasible and sustainable. As hydrokinetic technology continues to evolve, the development of innovative solutions like the SWS will play a crucial role in bridging the gap between current

capabilities and the untapped potential of riverine energy resources. This progress supports the transition to renewable energy and addresses the electrification needs of communities near freshwater bodies, contributing to global energy security and sustainability.

2.5 The need for hydrokinetic turbines

The energy sector over the past few decades has witnessed a widespread and consistent shift toward renewable energy sources, driven by the increasingly severe consequences of climate change from using sequestered carbon. In 2020, the total installed renewable capacity increased by almost 260 GW, led mainly by influential countries such as China, the USA, and several European countries [68]. The expansion of capacity was facilitated by a substantial yearly investment of around USD 303.5 billion in the renewable sector. Consequently, the proportion of renewable energy sources in worldwide electricity generation, as depicted in Figure 4, increased to 29%, with hydropower being the primary contribution [69]. The primary factors driving the rapid growth and prevalence of hydropower are its high energy density and the predictable movement of water streams. Furthermore, another aspect that contributes to the preference for hydropower is its cost per kilowatt-hour of energy produced, which is 5-7¢. This cost is competitive compared to the 5-8¢ for onshore wind, and cost-effective compared to the 10-14¢ for offshore wind and 12-20¢ for solar [70], [71]. There are over 58,000 hydropower facilities globally, collectively capable of generating approximately 1150 GW of power [72]. Based on the current development trend, the International Energy Agency estimated a potential increase in hydropower capacity of up to 2000 GW by 2050 [73].

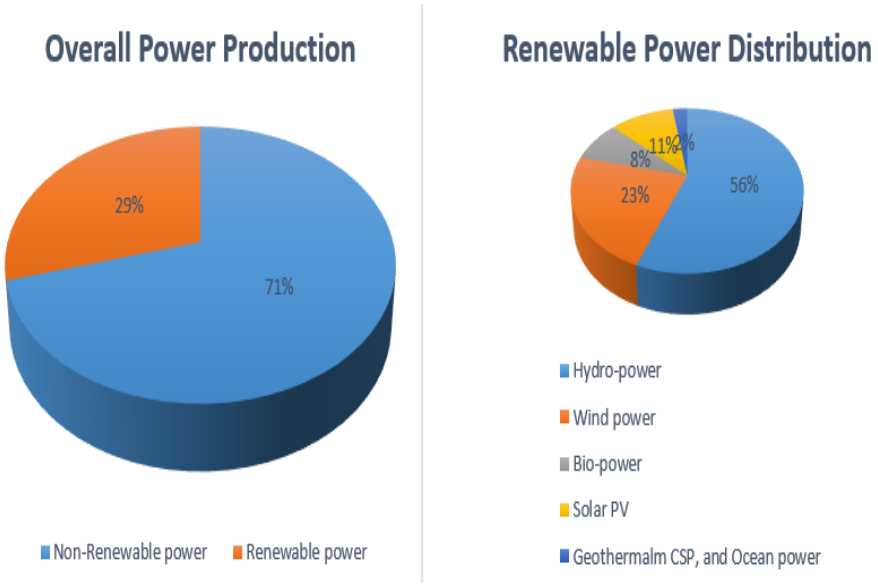

Figure 4: The estimated global production of renewable and non-renewable electrical power in 2020. The data highlights the significant contribution of renewable energy sources, which accounted for 29% of worldwide electricity generation, with hydropower being a major contributor. The move towards renewable energy is motivated by the need to lessen the effects of climate change and decrease dependence on fossil fuels. The expansion of renewable capacity was supported by substantial investments, amounting to approximately USD 303.5 billion in 2020, primarily led by countries like China, the USA, and several European nations [69].

Settlements like the Winnipeg River have access to flowing water, as shown in Figure 5. In most cases, the location is unsuitable for conventional high-head micro-hydro systems. More than 7.2 million people globally still need additional electricity access, and few people with access enjoy energy generated from fossil fuels. Behrouzi et al. [74] found that 33% of people worldwide have access to running water but do not have access to electricity. There are no economical, reliable, and easily implemented heat-killer thermoelectric generators for small power delivery for these people [41]. Some rivers have a low flow velocity; hence, some companies are working on low-speed turbines, as shown in Table 3. As investment in renewable energy continues to grow, RHKT systems like the SWS stand out as a viable and cost-effective option for enhancing global energy security and sustainability.

Table 3: List of some of the manufacturers of hydrokinetic turbines that have developed systems for river applications

No.	Device name	Manufacturer	Turbine type	Diameter (m)	Min/Max speed (m/s)	Output power
1	Free stream Darrieus Water Turbine	Alternate Hydro Solution Ltd. Canada	Cross-axis	2.5	0.8/it depends on the diameter	1 to 3-kW
2	Stream	Seabell int. co. Ltd (Japan)	Dual-cross axis	Data not available	0.6/no limit	0.5 to 10-kW
3	Gorlov helical turbine	Lucid Energy (USA)	Helical Darrieus turbine	1	0.6/no limit	Up to 50-kW
4	Water current turbine	Thropton Energy Service (UK)	Axial-flow propeller	1.8	0.5/it depends on the diameter	2-kW
5	DouGen	Electric Energy Ltd. (UK)	Axial flow propeller	0.31	0.9 to 4.1	100-W
6	SailGen	Electric Energy Ltd. (UK)	Axial/Horizontal	Data not available	3 to 4.1	125 to 280-W
7	Davidson Hill Venturi (DHV) turbine	Tidal Energy Pty. Ltd. (Australia)	Cross-flow turbine	1.5	1 to 2	0.77 to 6.16-kW
8	Current 025 Series	New Energy Corporation	Cross-axis	4.8	2.4 to 3	25-kW
9	EnviroGen 005 Series	New Energy Corporation	Cross-axis	1.5	3	5-kW

Figure 5: This top-view image showcases the CHTTC on the Winnipeg River in Manitoba. The facility is critical for testing and evaluating various hydrokinetic turbine designs under real-world conditions. The CHTTC provides a unique environment for researchers and developers to assess turbine performance, durability, and efficiency, contributing to advancements in riverine renewable energy technologies.

2.6 Commercially available RHKT systems

Areas that do not experience freezing temperatures are ideal for near-surface RHKT systems. The RHKT can work well throughout the year at 80% free-stream velocity. Tropical regions have monsoon rains that cause a rapid increase in mass flow rate in the river systems, hence the high velocity and presence of debris. However, surpassing the rated flow velocity may overheat the generator [75]. When the flow velocity is exceeded, the turbines can change the blade angle to adjust to the excess power. This can be achieved passively by letting the blade deform at increased velocity with the river current. Desired power can be achieved during high river flow close to the boundary layer zone when the rivers flood, mainly during monsoons and spring runoff. RHKT can operate using two rotors that cancel out the torque and make the system stand [76], [77], [78]. Although it is evident that RHKT systems are necessary, only a limited number of RHKT systems

are now producing electricity in rivers. The literature contains numerous studies that address innovative RHKT designs that have the potential to transform the hydrokinetic power supply industry. According to the literature, the commercially available RHKT systems are discussed below:

Mako axial flow turbine with a diameter of 2 m is appropriate for many applications such as tidal flows, rivers, irrigation canals, and tailraces. However, the price of a turbine with 2 m in diameter in 2020 varied between $20,000 and $70,000, making it a significantly costly investment [41]. In addition, the installation of such a turbine, as shown in Figure 6, requires a large river with more than two meters of depth.

Figure 6: A Mako axial flow turbine with a 2 m diameter featuring a horizontal river turbine design equipped with three rotor blades. The turbine's relatively large rotor hub is engineered to accommodate a low-speed generator, eliminating the need for a gearbox. This design suits various applications, including tidal flows, rivers, irrigation canals, and tailraces.

RHKT Archimedean screw-type invented by Jupiter Hydro is widely acclaimed as an economical and efficient technology. Shahsavarifard et al. [79] conducted trials and obtained a performance

coefficient, Cp, of around 0.45, which is remarkable given that it is more of a drag-type device. The prototype lacks precise pricing and figures. It claims that these arrays will be priced at one-third of the cost of its competitors. Figure 7 depicts a conceptual representation.

Figure 7: The deployment of an Archimedean RHKT at the CHTTC. The turbine features two counter-rotating screws, which can be inclined relative to the water flow to enhance overall water-to-wire efficiency. This innovative design aims to optimize energy capture from river currents, making it a promising solution for sustainable energy generation in riverine environments.

EnviroGen Systems, with a vertical axis design, have power capacities of 5 kW and 25 kW and are offered by New Energy Corporation of Canada. These systems have been globally implemented. These devices can be resized, with a range of possibilities from 5-kW to 250-kW [41]. Figure 8 illustrates a device at the CHTTC with a diameter of 1.5 m and blades measuring 0.75 m in length. This variant is specifically engineered to produce 5-kW of electricity in a current with a velocity of 3 m/s. To function when floating requires a minimum depth of 1.4 m, whereas fixed supports may accommodate a depth of 1.22 m. Furthermore, a low flow option measures 1.5 × 1.5 m and

produces 5-kW of power at a flow velocity of 2.4 m/s. This option necessitates a floating depth of 1.97 m or 2.15 m if fixed supports are used. The depth and velocity of the water current required to achieve the intended output suggest that this device is suitable exclusively for exceedingly large and swiftly flowing rivers when employed as a floating RHKT. Nevertheless, it might be used in narrower rivers by affixing it to stationary structures and impeding a substantial percentage of the water current.

Figure 8: A 5-kW vertical-axis turbine developed by New Energy Corporation mounted on a specialized floating support structure at the CHTTC. The structure is designed for easy transportation to the desired location, where it can be anchored securely to a shore anchor or a granite block on the riverbed. This setup allows for efficient energy capture from river currents, contributing to the advancement of hydrokinetic energy technologies.

GKinetic RHKT comprises two vertical axis turbines on opposite sides of the buoyant vessel. The vessel's shape amplifies the water's speed as it flows into the turbines. The exclusive blade pitch control system and the higher flow rate enhance power generation [41]. Figure 9 presents a diagrammatic depiction of this system in operation. It is claimed that the presence of slow-moving

water, which is often found in most deployment regions, can generate greater electricity. Nevertheless, the kinetic energy flux or power in a flow is constrained. It cannot be augmented unless the downstream level is diminished, resulting in the conversion of potential energy into kinetic energy. By boosting the velocity of the fluid movement around the obstruction, a larger quantity of energy becomes concentrated in the vicinity of the barrier while the total energy remains constant. GKinetic Energy [41] found that trees floating in a river in France were altered in their course. The system has a power output of 12-kW, a price of €78,000, and a weight of 1.9 tons. It would require the use of specialized lifting equipment for installation [41].

Figure 9: GKinetic's innovative vertical RHKT concept features two vertical rotors connected to micro-generators on either side. This design is engineered to harness the kinetic energy from flowing river water efficiently, enhancing power generation capabilities. The unique configuration of the vertical rotors allows for optimized energy capture, even in slow-moving water, making it a versatile solution for various riverine environments.

Ocean Renewable Power Company (ORPC) produced the RivGen underwater cross-flow helical turbine with two systems operating in Alaska [80]. The turbine shown in Figure 10 is a RivGen

being tested in Winnipeg River, Manitoba. Its design is to sink the turbine to function during the winter season. According to Thomson et al. [81], the mean water velocity in the river's main section at the ORPC deployment site in Iguigig is 2.5 m/s. Additionally, the authors observed substantial disparities in the rate at which fluid enters the turbine. While other RHKT systems are on the market, none are designed to operate in winter. Furthermore, they are unsuitable for depths shallower than 1 meter. Designers in nations with high labor expenses, such as Germany, Canada, and the USA, are physically distant from users in third-world countries and have traditionally struggled to create appropriate products for these regions. Typically, their designs are expensive, large, and have intricate implementation procedures. Furthermore, these devices frequently exhibit subpar performance in power generation since they are designed to operate optimally at flow velocities that are considerably greater than typical river velocities [81].

Figure 10: Before its submersion, the ORPC RivGen RHKT is being launched at the CHTTC on the Winnipeg River. The RivGen system is designed to generate renewable energy from river currents, providing a sustainable power solution for remote and off-grid communities. The deployment at CHTTC allows for comprehensive testing and evaluation of its performance and efficiency in real-world conditions.

Installing a diffuser downstream of a turbine reduces pressure at the turbine's rear end. This results in water entering the diffuser from a broader area than that covered by the turbine blades, enhancing power generation. Figure 11 displays the Guinard, 3.5-kW RHKT. The diffuser's wider diameter requires a greater depth, which leads to higher expenses and an increased likelihood of blockage from floating debris. Hence, its overall cost-effectiveness is arguable [41].

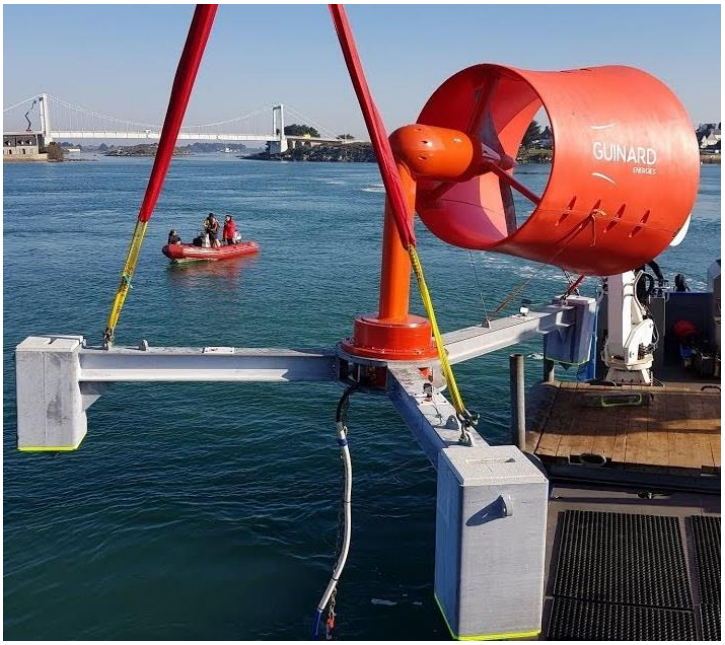

Figure 11: The Guinard 3.5-kW hydrokinetic turbine is designed to produce renewable energy in rivers and marine environments. It is engineered to harness energy from water currents, providing a sustainable power solution for various aquatic environments. The turbine is constructed using readily available off-the-shelf materials, making it a cost-effective option for small-scale applications.

Tan et al. [82] conducted a study in which they reviewed small RHKT systems and comprehensively described a prototype designed for shallow river applications. The prototype was constructed utilizing available off-the-shelf materials and cost under $300, not including labor costs. The item could be transported using a small pickup truck, while the power created from a

velocity of 1.26 m/s was 92 W. The potential to generate 2.21-kWh of electricity per day with a steady flow of 1.26 m/s may seem insignificant. Still, this quantity is sufficient to supply energy to a residence situated in a remote area, enabling the use of several direct current light bulbs and the recharging of a battery storage system. Although this prototype still needs further improvement, it demonstrates the kind of smaller-scale RHKT that can benefit remote villages.

While commercially available RHKT systems offer promising solutions for harnessing renewable energy from river systems, their adoption is often hindered by high costs, complex installation requirements, and limitations in cold climates. The current market offerings, such as the Mako axial flow turbine, Archimedean screw-type turbines, and vertical axis designs, demonstrate varying efficiency and adaptability. However, these systems often require significant investment and are best suited for large and energetic rivers. The challenges of ice formation and the need for specialized equipment further complicate their deployment in colder regions. The introduction of innovative designs, like the SWS, aims to address these issues by reducing costs, simplifying deployment, and enhancing performance in cold climates.

2.7 Riverine turbine challenges

The potential resources available in river environments such as those discussed above provide incentives for identifying the challenges of:

- problems inhibiting the adoption of RHKT,
- Cold climate impact on RHKT, and
- mounting arrangements and optimizing the positioning of the RHKT.

The research points to problems that lead to a reluctance to adopt RHKT systems. The LCOE is high; the hydro generator is impaired by ice in cold conditions, and the expense of adverse placement and retrieval procedures all affect RHKT performance [83], [84], [85]. Moreover, RHKT systems are exposed to air formation of an ice structure on the outside structure of the RHKT during winter. An ice layer that forms on the flotation system may impair the RHKT flotation system, causing the entire system to submerge [84], [86]. Kassam et al. [84], [87], [88] reported that the ice growth beneath the surface happens as frazil ice due to the water temperature, leading to frazil buildup in front of the turbine. Cold temperatures also affect the gearbox fluid. Ice accumulation on the structure exposed to air enhances weight along the mooring line, causing the turbine to submerge. These issues have increased the LCOE. Furthermore, the river has a boundary layer, which offers a dynamic region away from the riverbed. CHTTC conducted 40 non-dimensional measurements to determine the velocity profile of the river. The velocity profile shows that the river's surface is 95% of stream velocity. At the same time, the river depth is 35% of the river velocity. The velocity obtainable for a near-surface RHKT is 85% of the maximum velocity. The velocity achievable for a bottom-mounted RHKT is 60% of the V max. While the velocity profile is important, the speed variation over time is vital in deciding the energy obtainable in each place. CHTTC recorded the instantaneous velocity continuously for 104 hours. The maximum power density possible is 3,419 W/m^2, out of which the Betz limit allows only 59% to be extracted [89]. Turbulence causes continuous vibration to the system, reducing the internal elements' life span and resulting in the turbine's premature failure [90], [91]. Therefore, the proposed SWS offers energy cost reductions, has aerodynamic characteristics that can make operation easier in the water column, and can resist turbulence more than the other designs of RHKT systems.

Cold climate conditions pose substantial challenges to the operation and efficiency of RHKT systems, particularly due to frazil and anchor ice formation. Frazil ice forms in turbulent, supercooled water and consists of small disc-shaped crystals (1 to 4 mm in diameter) that can coalesce into larger formations like flocs or pans. These aggregations obstruct water flow and disrupt turbine operations, reducing power generation efficiency [86]. This phenomenon can reduce power generation by up to 30% in some hydro installations, such as the Riviere-des-Prairies plant in Quebec, and has been observed to lower river flow by up to 25%, as in the Niagara River [86]. Furthermore, frazil ice can block inlet vanes and accumulate around turbine components, particularly near the water surface, severely impeding power output. In addition to frazil ice, anchor ice poses a threat by attaching to riverbeds and reducing flow by 20 to 30%, creating further operational hazards for submerged infrastructure [38]. Ice cover and ice floes present significant risks to RHKT, as they can encase equipment and cause severe damage, particularly during the spring break-up of ice sheets. Several strategies, such as ice booms and forebays with ice covers, have been proposed to mitigate these issues by slowing water flow and promoting the rapid formation of stable ice cover, reducing the impact on water surface-mounted RHKT systems. However, operating hydrokinetic turbines in cold climates remains challenging and costly, with safety concerns further limiting the use of surface-mounted systems in such conditions. Deploying turbines below the water surface offers an alternative, but this approach is complicated by the lack of sufficient data to support its effectiveness in cold climates fully. Although necessary for survival in cold weather conditions, bottom-mounted turbines operate at lower velocities and require skilled personnel and boats for deployment, often over multiple days, significantly increasing the LCOE. These factors underscore the need for robust design and strategic deployment to mitigate ice impacts and ensure efficient power generation. The adoption of underwater RHKT systems, such

as the SWS, has become increasingly important, as it allows turbines to operate independently below the water surface, where seasonal temperature variations are relatively minor. However, reduced power density in bottom-mounted turbines, particularly during winter when flow rates decrease, can affect capacity factors.

RHKT systems face significant challenges due to ice formation in cold climates, which can lead to damage and operational issues. Ice formation is a critical issue for RHKT, particularly surface-mounted ones. The accumulation of ice on the turbine and its support structure, as shown in Figure 12, [92] can inhibit the operation of the turbine by increasing the weight and drag on the system and potentially leading to mechanical failure [35], [93]. In early winter, water can turn into frazil ice, which consists of loose, needle-like ice crystals. This type of ice can clog the turbine and inhibit its operation. The frazil ice can encase the turbine's shaft and prevent it from rotating [43]. Brijandi et al. [86] identified potential RHKT sites by observing the seasonal flow velocities and the patterns in the ice formation that make an opening in the ice surface during winter RHKT, as shown in Figure 13. During winter, the flow velocity of rivers decreases significantly, leading to a corresponding drop in power output, as the power generated by the turbine is a function of the flow velocity cubed [38]. Cold weather conditions pose additional operational challenges. For example, deploying and retrieving turbines in icy conditions can be hazardous and require specialized equipment and procedures, such as survival suits, as shown in Figure 12, to prevent hypothermia in case of accidental immersion in cold water. Regular maintenance and ice removal are essential to guarantee the functionality of a surface-mounted turbine in cold conditions. Nevertheless, safety rules frequently limit water operations in freezing conditions, resulting in a restricted operational time for RHKT in cold climates of around 6 to 8 months annually [38]. Thus, for RHKT systems

to be viable in cold climates, the SWS offers a promising solution by operating below the ice in the water column, avoiding ice accumulation, and maximizing power generation.

Figure 12: Challenges of a winter operation that inhibits regular procedures at the CHTTC: (left) floating support structure for the horizontal axis turbine is covered with snow, representing the ice accumulation on the pontoon, and (proper) survival suits are required for winter testing. If someone falls into the water, the suits will help to delay the onset of hypothermia but can do little if pushed below the ice cover.

Figure 13: The potential of the Winnipeg River for deploying surface-mounted RHKT, as it maintains openings in the surface ice even at temperatures as low as -40°C. These natural openings provide an opportunity for continuous energy generation during harsh winter conditions, which is crucial for maintaining power supply in cold climates. The ability to operate in such extreme temperatures underscores the adaptability and resilience of RHKT systems in northern regions.

2.8 Arrangement of RHKT mounting

Khan et al. presented three different methods. [33] for mounting RHKT, as shown in Figure 14, near-surface structure mounting (NSM), bottom structure mounting (BSM), and floating structure mounting (FSM). The authors thoroughly assessed multiple turbine systems, classifying and comparing them. Both axial and vertical flow turbines are specifically engineered to convert hydrokinetic energy. However, vertical flow turbines are particularly favored for their duct utilization. The Darrieus-type turbine is suitable for mooring and floating applications. It is imperative to select the rotor placement in the river carefully.

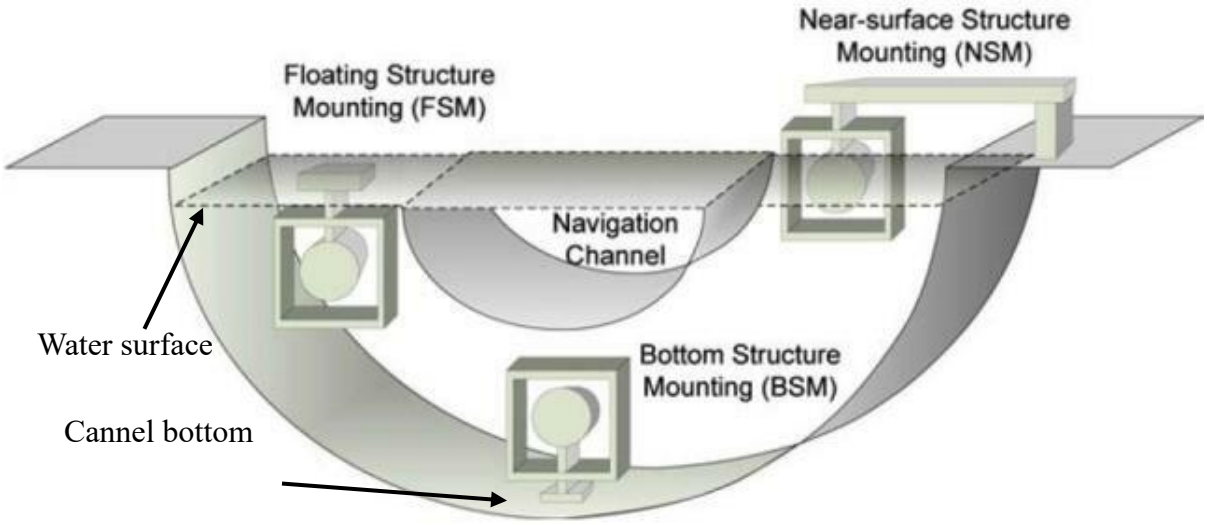

Figure 14: RHKT rotors can be strategically placed in three distinct locations within a river channel to optimize power extraction from flowing water. Each placement option is designed to maximize energy capture by considering water velocity, depth, and flow patterns. By analyzing these variables, engineers can determine the most efficient rotor positioning to enhance the overall performance and output of RHKT systems, contributing to more effective and sustainable riverine energy solutions.

The placement of the rotor in the river is vital when deciding where to position the RHKT. Thus, the following criteria should be considered:

- Multiple researchers have stated that cross-flow turbines are very suitable for river systems, as they do not necessitate water-sealing solutions for the producing equipment [94]. Thus, it is imperative to guarantee that they are situated at an elevated altitude relative to the water level. Therefore, the most favorable choices for mounting are FSM and NSM [33].
- Maximum energy extraction is at the upper surface when the flow velocity is maximum, for which the most suitable option for mounting would be the FSM system [33].
- Environmental degradation is directly associated with any disturbance caused by building or excavation on the riverbed. To promote environmental protection, either FSM or NSM methods should be adopted. Scouring at the riverbed will modify the flow regime, decreasing turbine efficiency [33].
- The NSM or BSM mounting option is allowed in areas of high sensitivity for navigating, fishing, and tourism vessels.

The understanding of floating structure design is far less extensive than the information available for surface-mounted structures. This challenges the increased use of alternative models such as FSM or NSM [94]. The installation, operation, and maintenance of BSM turbines present substantial problems. The placement of an RHKT in channels is generally influenced by two factors: (a) the energy flux is higher near the surface of a stream than at the channel bottom, and (b) this has implications for navigation, bridges, fishing vessels, and other activities. When constructing the RHKT in rivers, it is crucial to consider various factors, including water supply, topographical conditions, dam outlet openings, and fish habitats [33], [94]. Therefore, the SWS offers solutions for the problems above due to its ability to safely operate in the water column near the high energy flux and far from ice formation, boat traffic, etc. Therefore, the arrangement of

RHKT mounting is a critical factor in optimizing the performance and environmental compatibility of RHKT. The selection between near-surface, bottom, and floating structure mounting must consider factors such as energy extraction efficiency, environmental impact, and navigational safety. While floating and near-surface mountings offer advantages in energy capture and reduced environmental disturbance, their design and implementation challenges remain. The SWS emerges as a promising solution, addressing these challenges by enabling safe operation within the water column, optimizing energy capture, and minimizing interference with riverine activities and ice formation.

2.9 Economic analysis for RHKT

Brian Kirke [41] documented the limited number of organizations that disclosed cost information regarding RHKT. His results are replicated in Table 4 below. Only a limited number of systems last long enough to provide tangible results. Reviewing current technology poses a challenge because what is considered "current" at the time of writing will inevitably become outdated in a few years. Also, reviews over 10 years old hold less value when assessing pricing. An optimal approach is to examine illustrative instances that offer information such as cost, necessary depth, and design flow velocity for the desired result. However, the available literature provides limited valuable information regarding cost-effective RHKT.

Table 4: The estimated cost and the capacity of RHKT with the manufacturer companies in the market in March 2019

Company	Capacity	Cost in USD
Idenergie	500-W	$10,000
Greenenergy	183-W	$16,000
Hydrocat	40-kW	$75,000
ORPC	20-KW	Unknown
New Energetics USA.	1-kW	$8,500
	5-kW one-speed motor	$13,500
	10-kW two-speed motor.	$20,000
New Energy Corp Canada	5-kW vertical axis turbine, complete off-grid system	$50,000

The cost estimates incorporate data obtained from local South African wholesalers of generation equipment, as cited by Kusakana [36]The cost of an RHKT system with a power output of 1 kW is $7500. For a 7-kW diesel generator, the converter costs $1240, and the overall cost is $3,730. A 6-kW inverter is priced at $3,730. The battery, which has a voltage of 6 volts and a capacity of 360 ampere-hours, costs $215. According to Miller et al., the wind turbine, which has a power output of 7.5 kW, costs $26,900 [37], the cost of a bank of sixteen water-wheel river current turbines, each with a swept area of 10 m^2 and a river velocity of 0.3 meter/s, was projected to be $13,000. The concept involved using turbines that produce at least 500 watts apiece, which aligns effectively with a power output of 100 watts per turbine. The test cost includes $360 for materials and $4750 for installation, which covers site preparation. The labor cost per site is $1276. Free surface water wheels, often called stream water wheels, are the most efficient type of water wheel, with an effectiveness rate of approximately fifty to sixty percent [37]. However, it is unclear if the 10 m^2 swept area refers to a single turbine or the entire array. Each turbine would require a minimum area of 10 m^2, and a sufficiently large bank would be necessary to generate useful power. According to Emea et al. [95], a hydrokinetic turbine's output power is proportional to the flow

velocity. Consequently, the expense of installing it has significantly decreased from approximately $7,900/installed kW to around $2,500/kW.

Puertas-Frías et al, [96] analyzed the socio-economic viability of a hydrokinetic installation in two contrasting scenarios: a developing mixed economy, such as Brazil, and a major economic power like the USA. The study focused on an RHKT produced by Smart Hydro Power, designed for rivers and canals. This turbine has a 3-blade rotor with a 1-meter diameter and can generate up to 5 kW at a flow velocity of 3.1 m/s (with a power range of 0.25 to 5 kW and rotational speeds of 90 to 230 rpm). The turbine operates efficiently in mid-to-high discharge rivers, such as the Amazon in Brazil and the Mississippi in the USA. For example, in the Baton Rouge area, the Mississippi River has velocities ranging from 1 to 3.6 m/s, with an average velocity of 2.25 m/s [97], [98], Similarly, in the Itacoatiara municipality, the Amazon River experiences velocities between 1 and 2.5 m/s, with speeds exceeding 2 m/s for 211 days a year [99], [100].

Two levels of RHKT installations were evaluated: one with a power output of 3-kW and the other at 5-kW, corresponding to flow velocities of approximately 2.7 m/s and 3.25 m/s, respectively. Both scenarios assumed a similar power coefficient (CP ≈ 0.45), but a slightly reduced overall efficiency compared to earlier estimates due to energy losses during transmission from the turbine to a household. The overall estimated efficiency was about 85%, factoring in typical component efficiencies: gearbox efficiency at roughly 96%, generator efficiency at 90%, and transmission losses due to Joule heating at about 98% [101]. The turbine's initial investment is $14,988, and the generator and grid connection system is estimated to be $22,223 [102].

The annual income from the RHKT installation comes from two sources: (a) the electricity supplied to households and (b) the surplus energy sold to the power grid. The income from household electricity can be viewed either as energy savings for a cooperative of homeowners or as profit for an energy company. In 2020, the average electricity prices were comparable in the USA and Brazil, at $0.132/kWh and $0.121/kWh, respectively [103], [104]. Therefore, while the current literature on the cost-effectiveness of RHKT remains limited, the decreasing installation costs and the socio-economic analyses from diverse regions highlight their growing viability as a renewable energy source. The comparative cost analysis with traditional energy systems, such as diesel generators and wind turbines, underscores the potential of RHKT systems to offer competitive and sustainable energy solutions, particularly in river-rich areas. As technology advances and more data becomes available, RHKT systems are poised to become crucial in the global shift towards renewable energy, offering significant benefits for both developed and developing economies. This aligns with the SWS's goal of enhancing energy access and sustainability, especially for remote communities that can leverage their natural river resources.

2.10 Performance evaluation of RHKT

Golecha et al. [105] experimented to improve the efficiency of a modified Savonius rotor by adding a deflector plate on the blade side and increasing the phase rotation frequency. The main goal was to ascertain the optimal quantity of deflector plates on the phase with frequent blade rotation and assess the enhancement in blade performance on that side. The CP increased by 50% while the rotating phase was placed at the best possible location for a single-stage modified rotor. A single-stage modified Savonius rotor is the best solution, rather than two or three stages. Golecha et al. [105], [106] also examined the efficiency of a modified Savonius water turbine equipped with two deflector plates. The study's objective was to evaluate the most optimal position for the deflector

plate, which is positioned during the initial flow phase, to enhance the efficiency of the rotor power. By utilizing two deflector plates positioned strategically upstream of the flow, the maximum CP was increased to 0.35. Similarly, by employing a solitary deflector plate on the side where the revolving blade returns, the maximum CP reached 0.21, but the absence of a deflector plate yielded a CP of 0.14. Thus, in this scenario, utilizing the optimal placement of the deflector plates enhances the efficiency of the modified Savonius rotor.

Batten et al. [107] investigated the potential for increased performance efficiency in a floating free-stream energy converter by examining the design of a floating body structure. The empirical evidence indicates that the utilization of separators is a cost-effective approach to improve power generation. The study mentioned that the insertion of a 90° divider saw a nearly 100% increase in the power produced. There was only a slight increase in power when using a 45° separator. The insertion of a scoop at 45° raised the power generation close to that of the 90° separators. It is possible that a floating water wheel could be considered to generate electricity in small-scale operations in rural areas where the location of these constructions would be economically viable and construction costs would be low.

Thus, the performance evaluation of RHKT underscores the significant potential for efficiency improvements through innovative design modifications. The studies by Golecha et al. demonstrate that strategic placement of deflector plates can substantially enhance the efficiency of modified Savonius rotors, achieving notable increases in power coefficients. Similarly, Batten et al.'s exploration of floating free-stream energy converters highlights the effectiveness of structural modifications, such as separators and scoops, in boosting power generation. These findings suggest

that with continued research and development like the SWS, which can operate under ice layers in cold climates, RHKT can become increasingly efficient and cost-effective, particularly for small-scale applications in rural and remote areas.

2.11 Further methods for turbine performance enhancement

Various enhancement techniques are applied to increase the turbine power density in different situations [108]. It is also important to consider the turbine placement in the flow region, mostly when placed in an array to maximize the power generation, and while predicting the flow impacts of the turbine unit, the velocity zone distribution in the plan view is even [109]. Physical and numerical modeling experiments have been done to ascertain the enhancement approaches, and such information is demonstrably useful for running resourcefully. These works have limitations, such as reliance on the analysis as the methodology. Field experiments rarely verify the systems as these are difficult and expensive to perform at scale. The consideration of overall drag increase, which influences the cost of high turbine anchoring and orientation in the debris, may not be appropriate for all uses, which should be analyzed in an economic assessment [67], [108].

In the context of this research, the focus is on developing and testing a SWS to enhance the deployment and operation of RHKT in cold climates. Various hydrokinetic turbine designs exist, with the turbine concept being the most prevalent for river applications, commonly referred to as River Current Turbines or River Current Energy Conversion Systems [33], [66]. Among these, horizontal axis turbines dominate global research and development, accounting for 76% of efforts due to their ability to self-start even at lower water velocities. However, they are prone to clogging and higher energy production costs [110]. Vertical axis turbines, with rotors perpendicular to the water plane, offer installation costs and operational flexibility advantages, as they do not require

yaw mechanisms [111]. Crossflow turbines, characterized by their rotor axis parallel to the water surface, are particularly suited for hydrokinetic farms due to their spatial efficiency and reduced environmental impact, operating at lower speeds to minimize cavitation and noise [112].

3 SWS design and methodology

The methodology for the proposed SWS design is presented, focusing on the design stability, deployment, retrieval, and operational procedures using the following approach:

a) design an SWS structure for the RHKT prototype scale model using the open-source Xflr5 software and test the static and dynamic stability,
b) design and build an SWS prototype scale model using 3-D modeling,
c) 3-D print the SWS prototype scale model and prepare it for the water tunnel test,
d) test the stability of the SWS prototype scale model in the water tunnel and
e) build a larger prototype to be tested later.

The SWS design necessitates the integration of multiple components to meet the research objectives and ensure efficient operation in the water column. A two-bladed rotor with blades placed at 3 and 9 o'clock enables the turbine to easily float close to the riverbank at a depth of approximately less than 1 m to reduce deployment and retrieval costs. Such an arrangement allows the deployment of the SWS from a trailer at the riverbank to eliminate the need for onsite lifting equipment. Placing a turbine far from the riverbank remains challenging as the maximum lifting load decreases rapidly with distance for any crane design.

The SWS prototype scale is designed for 3-D printing, with reinforcement rods to connect the wings and fuselage in the prototype scale model. Functional components must ensure the SWS remains stable in the water column, thus incorporating tail and dihedral angled wings to address known field stability problems. The design technique requires the SWS to maintain a positive AOA

throughout deployment and retrieval. To achieve its operational depth, the system needs a negative AOA after positioning the SWS in the water column, and it should transition to a positive AOA to start operating. The SWS must operate stably and overcome floating ice and debris to avoid damage.

Creating and testing a SWS prototype scale turbine is thus critical to achieving objectives. This turbine must undergo testing in the controlled environment of a water tunnel and the challenging conditions of an energetic river, specifically downstream of CHTTC at the Winnipeg River. It must address numerous severe design challenges to ensure effective deployment and consistent stability, meeting the requirements for year-round operation within this highly dynamic riverine system. For this work, testing is limited to the water tunnel only.

To address the design challenges associated with designing a SWS for effective use and stability in a river environment, the following steps are operationalized:

- Design a RHKT system that can fit onto a trailer for easy deployment from a riverbank.
- Develop a RHKT system for easy deployment in the water column at various depths.
- Designing an SWS prototype structure for an RHKT that can submerge and operate effectively within the water column, addressing challenges related to maintaining operational stability amidst fluctuating large flow structures and water conditions.

Designing and testing an SWS involves several steps, from the initial design using Xflr5 and SolidWorks to 3-D printing the model and conducting water tunnel tests. The steps are as follows:

1: Preliminary design and analysis using Xflr5:

a) Aerodynamic profile selection: When selecting an appropriate airfoil for the aircraft, consider the SWS's intended purpose and performance requirements.
b) Geometry design: Create the geometry in Xflr5 by specifying parameters such as wingspan, wing area, aspect ratio, and tail design. This software enables 2-D and 3-D visualizations of the SWS.
c) Aerodynamic analysis: Use the Xflr5's tools to predict SWS performance characteristics, including lift, drag, and stability, which is crucial for refining the design.

2: Detailed 3-D design using SolidWorks:

a) 3-D modeling: Transfer the SWS design from Xflr5 to SolidWorks, creating a detailed 3-D model of the SWS, including the fuselage, wings, tail, and other components.
b) Component integration: Ensure precise integration of all components into the 3-D model.

3: Exporting SWS to 3-D printer:

a) File preparation: Export the SWS design to STL file format, ensuring proper scaling and orientation for printing.
b) Material selection: Choose a suitable 3-D printing material based on SWS requirements.
c) 3-D printing: Use a 3-D printer to build the prototype scale SWS, ensuring precision and high quality to maintain design accuracy.

4: Water tunnel testing:

a) Preparation: Prepare the 3-D printed SWS prototype scale for water tunnel testing by assembling all parts, adding instruments for data collection, and securely mounting the model in the water tunnel.
b) Data collection: Conduct water tunnel tests, measure aerodynamic stability, and record and analyze the data obtained.
c) Iterative design: Refine the prototype scale SWS design based on test results, adjusting components such as wing shape, control surfaces, or weight distribution to optimize performance.

5: Final analysis and conclusion for the tested SWS prototype scale: Analyze water tunnel test data using open-source Tracker software and Excel, then convert to MATLAB for comparison with previous SWS prototype scale models. Evaluate the prototype scale SWS performance and its suitability for its intended purpose.

Accordingly, the design and methodology of the SWS for RHKT represent a significant advancement in addressing the challenges of deploying and operating turbines in dynamic river environments. By leveraging open-source software like Xflr5 for aerodynamic analysis and employing 3-D modeling and printing techniques, the SWS design aims to enhance stability and operational efficiency. The innovative approach of using a two-bladed rotor and dihedral angled wings ensures that the SWS can be easily deployed from a riverbank, minimizing the need for heavy lifting equipment and reducing costs. The focus on maintaining a positive angle of attack during operation and transitioning to a negative angle for deployment highlights the system's adaptability to varying river conditions.

3.1 Xflr5 design

In this study, a significant change was implemented in the previous SWS model, which used the NACA 2412 and NACA 0018 airfoils. The update involved switching to the NACA 0012 airfoil with a dihedral angle, inspired by the Boeing 737-Max airplane. This modification was anticipated to affect the SWS stability characteristics positively. Wing dihedral angle refers to the upward angle from the horizontal plane of an aircraft's wings and is measured between the wing's chord line and the horizontal plane. The angle is essential for ensuring lateral stability as it enhances roll stability. A positive dihedral angle, where the wingtips are higher than the wing roots, improves the aircraft's ability to return to its flight level after a disturbance [113]. The geometric characteristics for the NACA 0012 airfoil, as shown in Figure 15, were systematically collected from the Airfoil tool database and incorporated into the Xflr5 software platform to facilitate this transition. In river applications, the flow characteristic length scale can be many times larger than the turbine place cord, as an event by river boils seen at the surface, which can measure over 10 m at energetic river sites.

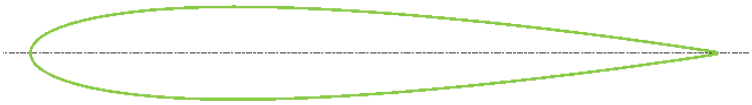

Figure 15: The use of the NACA 0012 airfoil in the development of the new SWS prototype model, which incorporates a dihedral wing and a tail. The NACA 0012 airfoil, known for its symmetrical shape and aerodynamic efficiency, is selected to enhance the stability and performance of the SWS. These design modifications are crucial for optimizing the SWS's operational capabilities in river environments, where maintaining stability is essential for adequate energy capture.

After studying the pressure distribution on the NACA 0012 wing, both lift and drag can be determined. However, it is important to recognize that the pressure distribution is influenced by the airfoil shape, the AOA, and Reynold's number (Re). The force acting on the airfoil results from three types of drag: lift drag, induced drag, and profile drag. This force can act at any point of the chord and causes the aircraft to pitch up or down.

The lift, drag, and moment are expressed as dimensionless coefficients, which are dependent on dynamic pressure, $q = \frac{1}{2} \rho v^2$, where ρ is the fluid density and v is the flow velocity given as:

$$Cl = \frac{L}{q A} \qquad (3)$$

$$Cd = \frac{D}{q A} \qquad (4)$$

$$Cm = \frac{M}{q A c} \qquad (5)$$

$$\text{Aspect Ratio} = \frac{S}{c} \qquad (6)$$

Where, L is the lift force, D is the drag force, M is the pitching moment, A is the wing area, s is the wingspan, and c is the wing chord, which is included in the equation of C_m to make it dimensionless. It is known that aircraft employing higher aspect ratio wings are aerodynamically beneficial to the reduction of induced drag [114]; however, the aspect ratio wings in this study are limited to the water tunnel dimension.

The dimensions of the wings and tail and the exact separation distance between them are specified to ensure the structural integrity and balance of the SWS in the water environment. Moreover, the distribution of masses across various SWS components, as shown in Figure 16, is built on insights from the previous tailless model. The mass of the selected motor was measured and combined with the tail mass. In contrast, the mass of the mooring line was incorporated to maintain the equilibrium of buoyancy, center of mass, and center of pressure. Additionally, three different dihedral angles were designed, as shown in Figure 17, to investigate which angle provides the greatest stability.

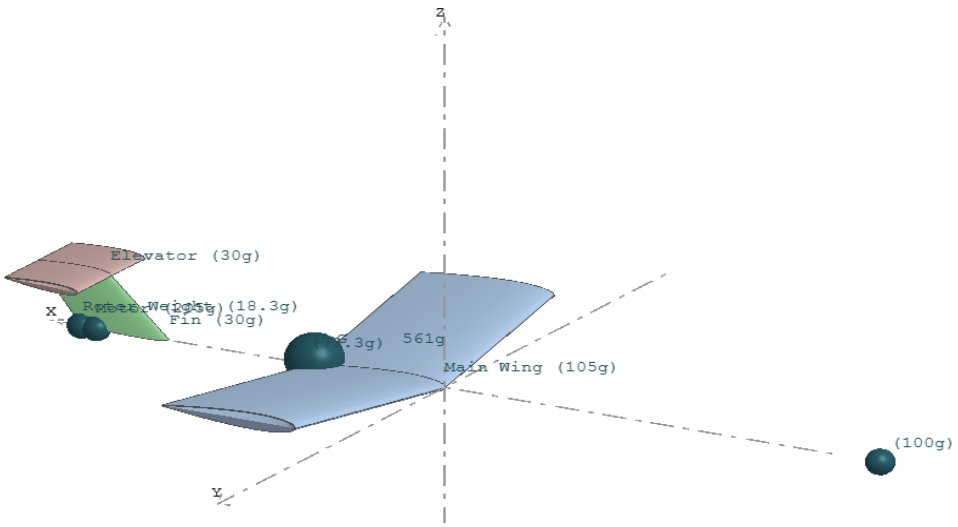

Figure 16: The mass distribution across the new SWS prototype scale model's components was analyzed using Xflr5 software during the initial design stage. The mass distribution is a critical factor in ensuring the stability and performance of the SWS. By strategically aligning the center of gravity, mass, and pressure points along a common axis at two-thirds of the airfoil's wingspan width, the design aims to enhance stability and control. This careful consideration of mass distribution is essential for optimizing the prototype's aerodynamic efficiency and operational effectiveness in dynamic river environments.

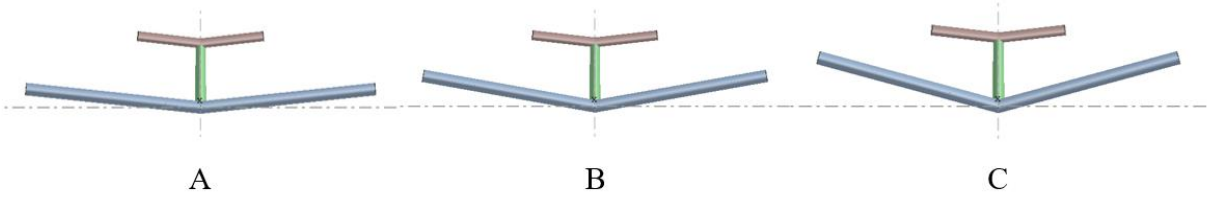

Figure 17: The SWS prototype scale models are each designed with different dihedral angles: (a) 6°, (b) 10°, and (c) 15°. These variations in dihedral angles are critical for assessing the models' stability and aerodynamic performance.

Determining lengths and mass distributions is a critical aspect of this investigation. The center of gravity, mass, and pressure points are intentionally aligned along a common axis at two-thirds of the airfoil's wingspan width. Specific design features, such as 6°, 10°, and 15° dihedral angles in the wings and a 14° offset towards the tail, are incorporated to enhance stability. The tail is

constructed using vertical and horizontal segments adhering to the NACA 0012 airfoil type, reflecting the characteristics of the wings and simplifying manufacturing.

Following the establishment of design specifications, a series of tests was conducted. These tests included static and dynamic stability assessments performed in Xflr5 using a water tunnel environment. The fluid density was set as water density. The velocity was adjusted from 0.5 to 1 m/s, corresponding to the flow velocity range at which the SWS prototype scale is tested in the water tunnel. Testing aimed to evaluate the SWS prototype scale's performance under simulated operational conditions, providing insights into its behavior within the specified aquatic environment.

3.2 SolidWorks design

The initial stages of the design process are conducted using SolidWorks, which facilitates the design work. Upon completing the design process in Xflr5, the airfoil data is imported from the Xfoil tools database to SolidWorks. This step must maintain the airfoil's precise geometry and safeguard against design flaws. The previous SWS model featured wings with a 14° offset toward the tail, was tailless, and had no dihedral angle, as shown in Figure 18. The new SWS model is designed with wings that also feature a 14° offset towards the tail, but it also includes a tail and a dihedral angle, as shown in Figure 18. The new SWS wings have dihedral angles of 6°, 10°, and 15°, respectively. This multimodal approach is intended to test the wings in a water tunnel at varying flow velocities. Wings are designed to deliver hydrodynamic performance in the aquatic environment, with a significantly higher fluid density than air. Additionally, small fins are placed at the midspan of each wing, serving a dual purpose. As shown in Figure 18. These fins contained hollow rings for mooring line cable connections for the harness and acted as reinforcement for the

SWS. The fuselage is an important component of the SWS design and features a square cross-sectional area, as shown in Figure 19.

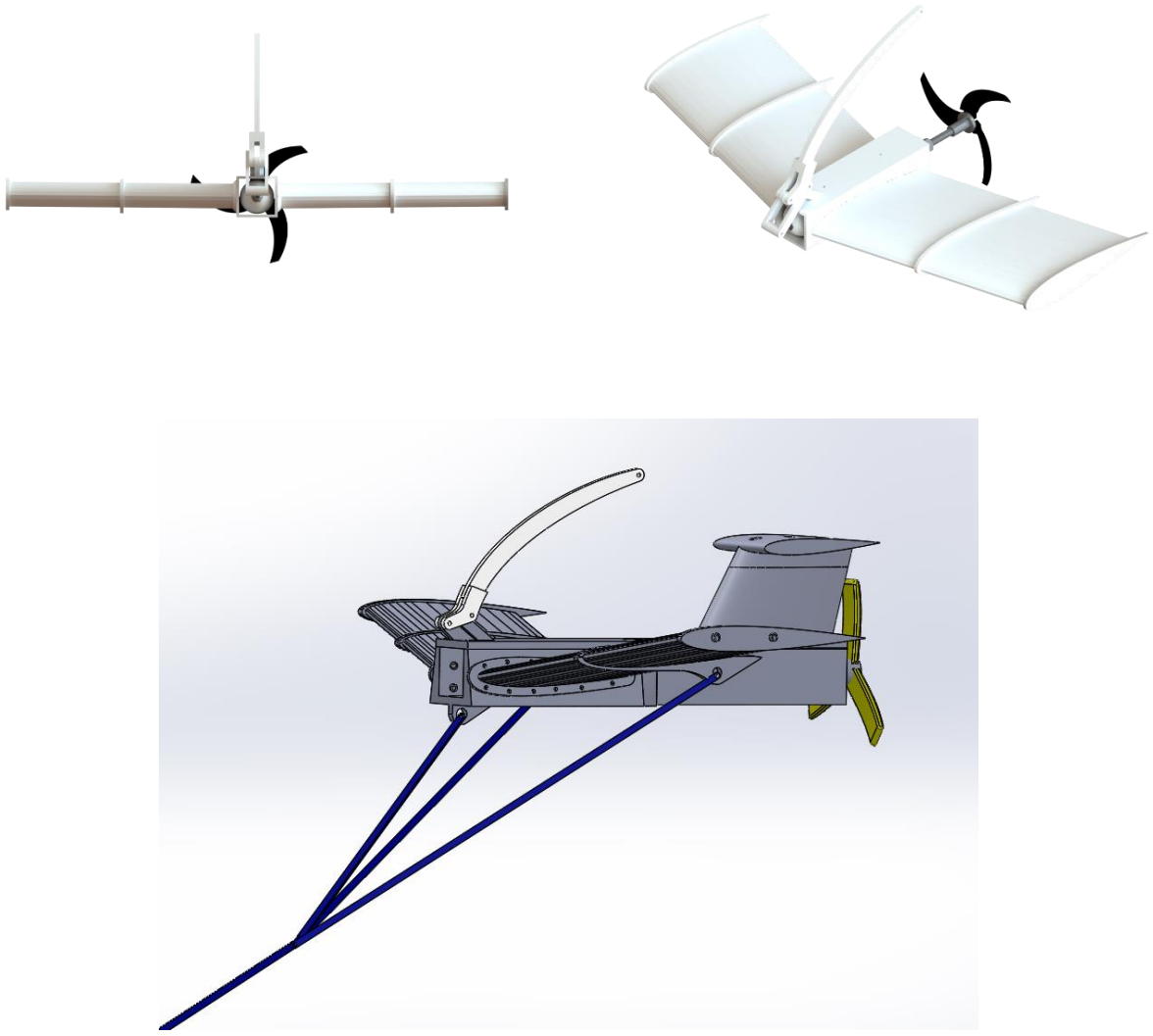

Figure 18: This is a comparative visual analysis of the SWS prototype scale models. The top section displays the front and 3-D views of the previous SWS prototype, highlighting its design features and structural layout. The bottom section presents a 3-D view of the new SWS prototype scale model incorporating a 6° dihedral angle. This updated design includes a harness connection, enhancing the model's stability and control. The dihedral angle is a critical modification to improve aerodynamic performance and operational efficiency in water environments.

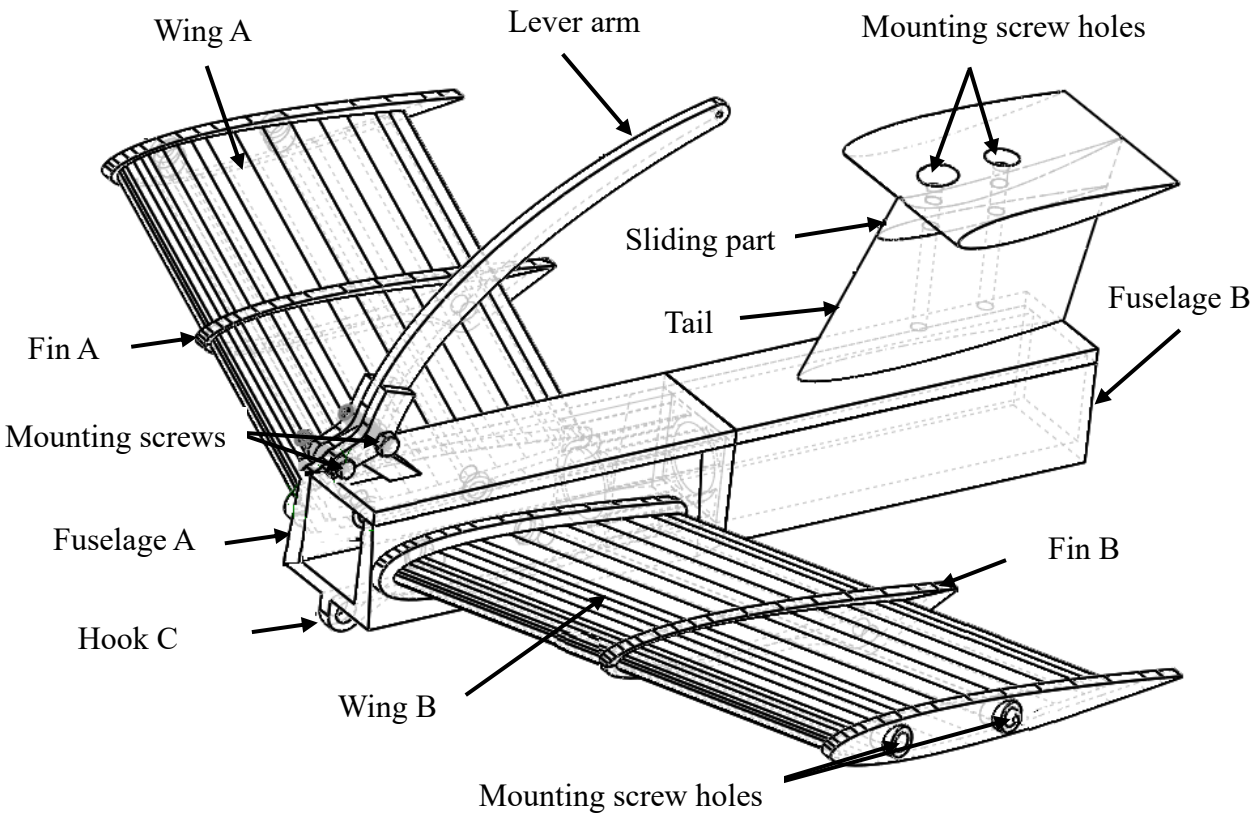

Figure 19: This schematic illustrates the SWS prototype scale model assembly featuring a 6° dihedral angle. The diagram provides a detailed view of the model's components, highlighting the integration of the dihedral wings, fuselage, and tail assembly. The design ensures smooth water flow, directing it efficiently toward the turbine blade in larger-scale models.

This design choice ensures smooth water flow, ultimately directing it toward the turbine blade in the larger-scale model. The fuselage includes two hooks at the nose, each serving a specific purpose. The upper hook has two hook connections for anchoring the arm that connects with the SWS, while the lower hook is for attaching the mooring line cable, as shown in Figure 20. Additionally, a midspan connection point is incorporated to allow dynamic adjustment of the tail position, which can be altered to be either an upward or downward orientation relative to the wings. This adjustment is facilitated by a press-fit hollow box positioned within the fuselage, as shown in Figure 20, to enable this control.

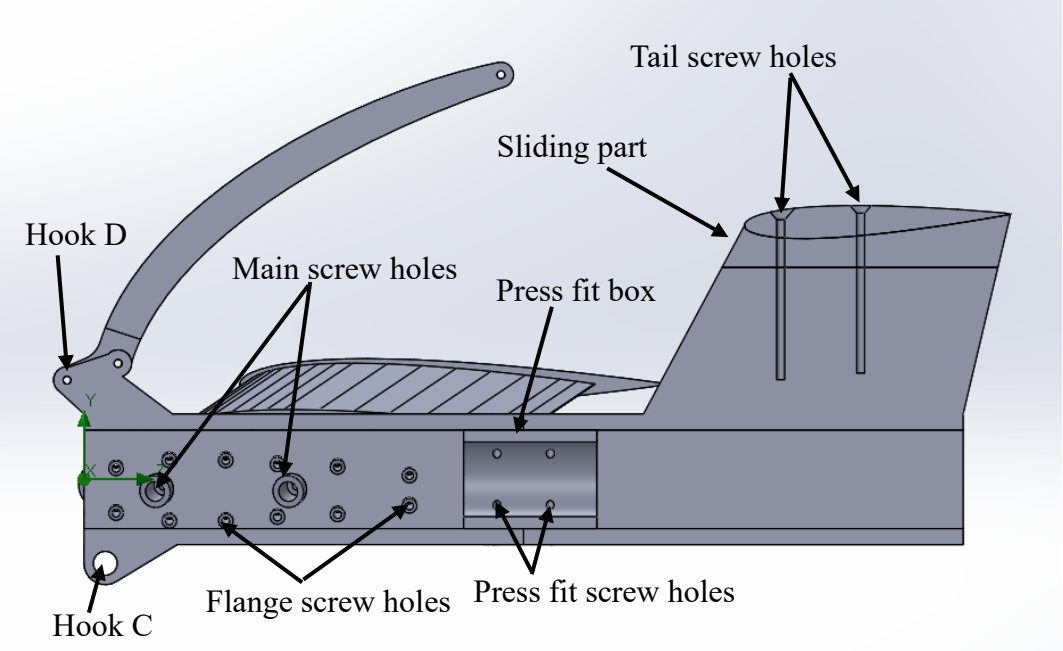

Figure 20: A detailed view of the fuselage, highlighting the wing flange and the press-fit box designed to hold fuselage parts A and B securely. The design includes hooks D and C, integral for attaching the lever arm and mooring line. Additionally, the figure showcases the sliding part of the tail, which is engineered to enhance stability and control by allowing adjustments to the AOA.

The lever arm features two hollows for attachment to the SWS through the top fuselage hook D and is constructed with a slight bend towards the tail. This arm controls the SWS buoyancy and attitude. The AOA can be adjusted by moving the arm forward or downward. Shifting the arm forward applies pressure to the nose, decreasing the AOA, reducing lift, and temporarily increasing drag. This leads to an essential maneuver for initiating a descent beneath the water's surface. Conversely, moving the arm downward increases the AOA, increasing lift and decreasing drag, which allows the SWS to resurface, as shown in Figure 21. Additionally, a cable connects the end of the lever arm to a drogue, a floating buoy on the water's surface, ensuring constant tracking of the SWS's position during operations. Drogue is critical for the retrieval of the SWS as it allows the surface of the turbine where it acts as a transport vessel again.

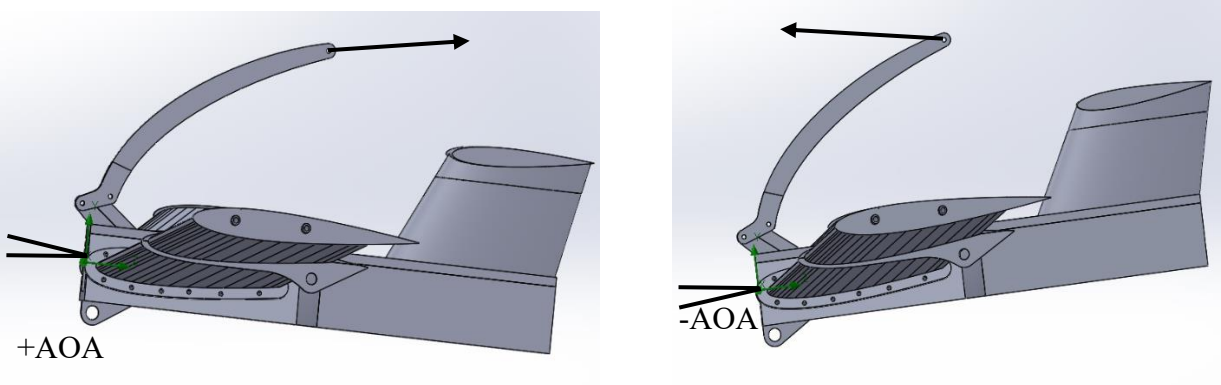

Figure 21: The operation of the drag system is crucial for controlling the AOA of the SWS prototype. In panel (a), moving the lever arm backward results in a positive AOA, which increases lift and decreases drag, allowing the SWS to ascend or maintain its position in the water column. Conversely, panel (b) shows that moving the lever arm forward creates a negative AOA, reducing lift and increasing drag, which facilitates the descent of the SWS beneath the water's surface.

The SWS's tail is engineered to serve as a stabilizing force, ensuring the SWS remains stable throughout its operation. This T-shaped tail design enhances the SWS stability by minimizing the drag created by the wings. A small sliding component in the middle of the vertical part of the tail is designed to maintain a positive AOA when the tail is positioned up or down. This movable component could be removed in a tail-down configuration to ensure a positive correct AOA for the tail, as shown in Figure 22. Two metal screws secure the two tail segments, including the small sliding component, starting from the top surface of the horizontal piece, passing through the slide, and ending at the midspan of the vertical part. This precise design approach ensures the SWS's stability, control, and accurate maneuverability during its operational life. The end goal is to operate the SWS, possibly without a tail, to simplify operations and manufacturing.

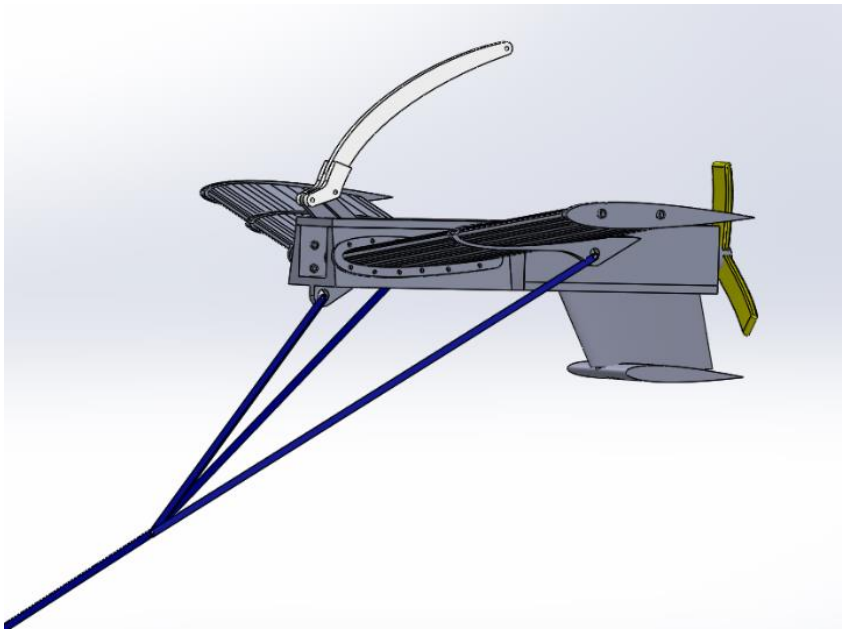

Figure 22: The SWS prototype, with its tail positioned downward, was achieved by adjusting the sliding part of the tail to maintain a positive AOA. The tail's design, which includes a movable component, allows for precise adjustments to ensure optimal performance in varying aquatic conditions.

The integration of SolidWorks into the design process of the SWS prototype has facilitated the development of a hydrodynamically efficient system. By incorporating a tail and varying dihedral angles, the new SWS model addresses the stability challenges faced by its predecessor. The strategic placement of small fins and the innovative fuselage design ensure smooth water flow and enhance the system's overall performance. The lever arm and drogue mechanism provide dynamic control over the SWS's buoyancy and attitude, allowing for precise adjustments in the AOA. This comprehensive design approach not only improves the stability and maneuverability of the SWS but also simplifies its operation and manufacturing.

3.3 3-D printing

The selected material for 3-D printing, chosen for its availability and suitability, is 2 kg of Polyethylene Terephthalate Glycol (PETG) filament. This amount was sufficient for producing the three SWS prototype scale models with dihedral angles of 6°, 10°, and 15°, respectively. The Bambu Lab P1S, as shown in Figure 23, was utilized to print these SWS prototype scale models.

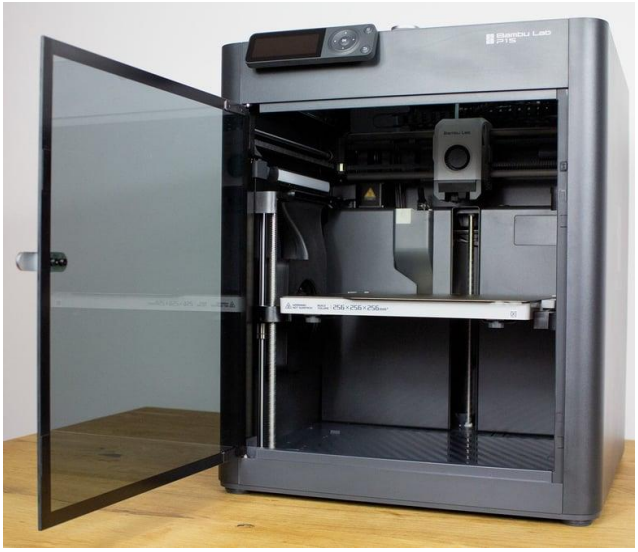

Figure 23**:** After the CAD design stages were completed, the Bambu Lab P1S 3-D printer was employed to fabricate the SWS prototype scale models. The printer utilized PETG filament, chosen for its durability and suitability for producing models with varying dihedral angles of 6°, 10°, and 15°.

The use of PETG filament in the 3-D printing process has proven to be a practical choice for fabricating the SWS prototype scale models. The material's availability and suitability ensured the successful production of models with varying dihedral angles, which is crucial for testing hydrodynamic performance. The employment of the Bambu Lab P1S printer facilitated the precise and high-quality construction of these prototypes, laying a solid foundation for subsequent water tunnel testing and further development of the SWS design.

3.4 Water tunnel testing

3.4.1 Testing preparation

The 3-D-printed SWS is prepared for water tunnel testing, which involves several steps. These include sealing all openings, adding data collection instruments, and ensuring the model is securely mounted. Various tests are conducted according to the experimental objectives highlighted earlier and detailed in the following sections to achieve satisfactory results.

The experiments conducted in the water tunnel utilized flow velocities ranging from 0.5 to 1 m/s. This range was selected to test the stability and performance of the SWS under controlled conditions, allowing for detailed observation of its behavior at different flow rates. The water tunnel provides a consistent and repeatable environment to assess the system's response to changes in flow velocity. In contrast, natural river environments can exhibit a broader and more variable range of flow velocities, often exceeding those tested in the water tunnel. River velocities can vary significantly depending on factors such as river size, gradient, and seasonal changes, with some rivers experiencing flow velocities well above 1 m/s. This variability challenges scaling the results from the water tunnel to real-world applications. Scaling laws and similarity principles must be applied to bridge the gap between the controlled water tunnel experiments and natural river conditions. The Reynolds number is a critical parameter in this analysis. The experiments in the water tunnel achieved Reynolds numbers in the range of (4.04 to 6.74) x 10^5. For accurate scaling, the Reynolds number in the water tunnel should match or be comparable to those in natural river conditions to ensure dynamic similarity. The scaling analysis underscores the need for further testing and validation of the SWS in environments that closely mimic natural river conditions. By ensuring that the system can operate efficiently across a broader range of velocities, the research

supports the hypothesis of developing a robust and adaptable RHKT system that can reduce the LCOE while maintaining environmental sustainability.

The SWS must be equipped with a mooring line to stabilize the entire system against the water flow during operation, as depicted in the schematic shown in Figure 24. The test also involves conditions related to the mooring line length, as detailed in Table 5. In addition, the model's wingspan, the distance between both end flanges of the wings, is used as a basis for scaling. As shown in Table 6. Due to the water tunnel dimensions, the span was scaled from 22 cm (Xflr5 design) to 11 cm in the 3-D-printed prototype for better movement space, resulting in a scale-down factor of 0.5.

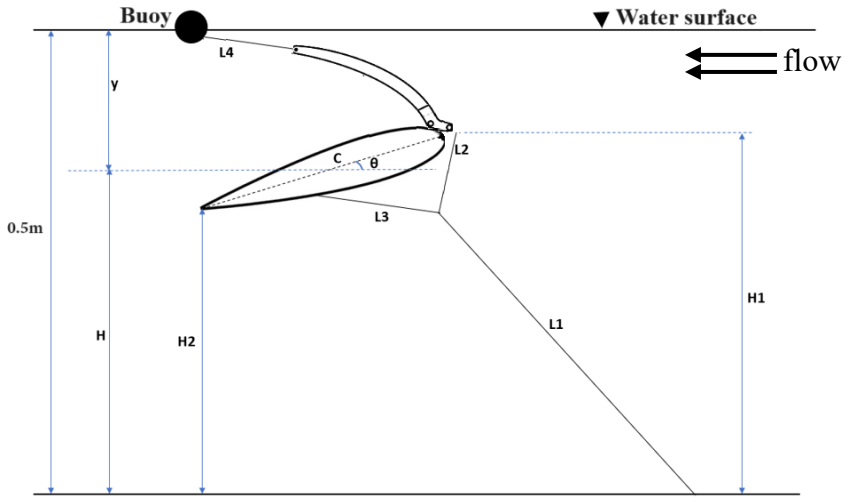

Figure 24: This schematic illustrates the relevant dimensions of the new SWS prototype scale model designed for water tunnel testing. It also highlights the placement of mooring lines and anchor points, which are crucial for stabilizing the model during testing.

Table 5: Mooring line length test conditions with the velocity range for the SWS testing stage

V	0.5 – 1 m/s
Le1	55 cm
Le2	10 cm
Le3	20 cm
Le4	30 cm

For each reference, the following symbols will be used to represent important dimensions of the model:

- H1, height from the base of the tunnel to the leading edge of the end flange
- H2, height from the base of the tunnel to the trailing edge of the end flange
- y, depth of submersion below the water surface
- H, the height of the turbine above the base of the tunnel, (H1+H2)/2
- Ch, chord length of the end flange, 6.5 cm for the SWS prototype scale
- Le1, length of the anchor rope
- Le2, length of the rope from linkage to knot
- Le3, length of the rope from wing to knot
- Le4, length of the buoy rope
- θ, the pitch angle of the wings where:

$$\theta = \sin^{-1}\frac{H1-H2}{Ch} \qquad (7)$$

Table 6: The dimensions of the Xflr5 design and the 3-D printed prototype used in the water tunnel experiment

Xflr5 design dimension		3-D printed prototype design dimension	
Wingspan	22 cm	Wingspan	11 cm
Wing chord	13 cm	Wing chord	6.5 cm
Horizontal tail span	8 cm	Horizontal tail span	4 cm
Horizontal tail chord	10 cm	Horizontal tail chord	5 cm
Vertical tail height	7 cm	Vertical tail height	3.5 cm
Fuselage length	33 cm	Fuselage length	16.5 cm
Fuselage cross-sectional area	4×4 cm	Fuselage cross-sectional area	2×2 cm
Scale-down factor	**0.5**		

The experiment in the water tunnel shown in Figure 25 illustrates the model's placement inside the water tunnel. Two mooring lines are mounted on the midspan of the wing on the third quarter of the wing chord, aligning with the center of mass, gravity, and buoyancy. These two lines are connected at specific lengths with the third line, which is attached to the bottom hook of the SWS's nose. These three lines converge into a single line extending to the anchor mass.

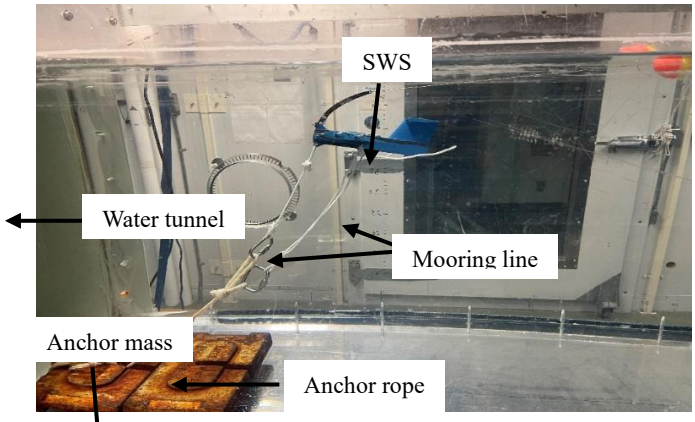

Figure 25The water tunnel experiment with the SWS prototype scale model featuring a 6° dihedral angle demonstrates its operation within the water column. The experiment highlights the model's stability and maneuverability by strategically placing mooring lines and anchor points. These lines are mounted on the midspan of the wing and converge into a single line extending to the anchor mass.

3.4.2 Data collection

Aerodynamic stability is tested during the water tunnel tests and recorded using a high-quality SIYI A8 camera (Shenzhen Baichen Trading Co., China), which takes 4K ultra-HD video & photography with 8MP 1/1.7inch, 320-degree yaw axis rotation and 6X digital zoom. The videos are then exported to Tracker software, which analyzes the stability data obtained during the testing process, as shown in Figure 26. The Tracker software divides each second of the video into 60 parts, and each part shows coordination to the X-axis and Y-axis for the selected point at the wing tips. This software is accurate in tracking the points, providing precise stability measurements. This analysis is performed twice for each video, once for each wing tip of the SWS. The data collected from this software is then exported to Excel and MATLAB to combine and plot the stability graphs.

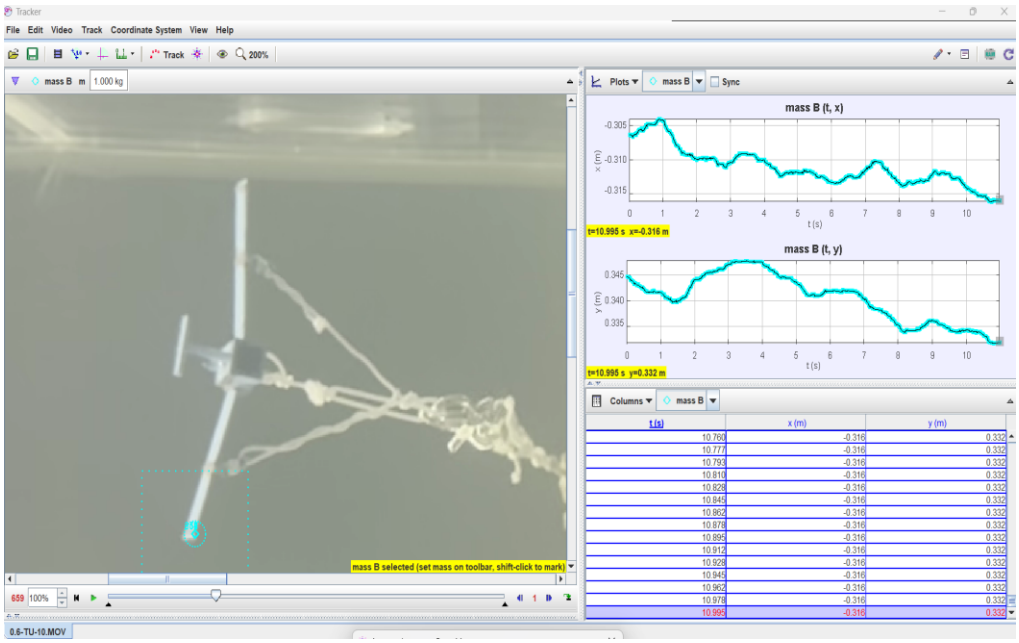

Figure 26: The analysis of recorded videos using Tracker software to measure the movement of the SWS prototype along the X-axis and Y-axis through remote sensing. The software divides each second of the video into 60 parts, providing precise coordination data for the selected points at the wing tips.

In standard settings, the precision of Tracker in analyzing videos is determined by several key factors that users must configure to ensure accurate measurements. Calibration is important for converting pixel measurements into real-world units. Users use a calibration stick or point pair to set a known length within the video as a reference. This step ensures that the scale of the video is accurately represented, which is essential for precise measurements of distance, speed, and acceleration. Setting the reference frame involves defining the origin and angle of the coordinate system. This setup aligns the coordinate system with the analyzed motion, vital for accurately tracking the object's movement across frames. The data collection process for the SWS prototype's aerodynamic stability testing is comprehensive and precise, leveraging advanced tools such as the SIYI A8 camera and Tracker software. By meticulously analyzing video footage and converting the data into detailed stability graphs through Excel and MATLAB, the process ensures high accuracy in assessing the SWS's performance.

3.4.3 Experimental procedure

Two cameras are positioned in the front window of the water tunnel, facing the flow, to record videos of the SWS prototype scale behavior during the testing process. Moreover, a variable-frequency drive (VFD), as shown in Figure 27, starts and stops the flow in the water tunnel by manipulating the frequency delivered to the motor. 72 statistically independent videos have been recorded and analyzed using Tracker software. Additionally, as shown in Table 7, specific parameters are required to obtain accurate results.

Table 7: Parameters were considered during the SWS prototype scale test in the water tunnel experiment

H_w: Water depth	0.5 m
μ: Dynamic viscosity	9 x 10^{-4} m^2/s
V: Freestream velocity	0.5 to 1 m/s
Re: Reynolds number	(4.04 to 6.74) x 10^5
Ma: Anchor mass block	25 Kg
Ar: Anchor rope	0.5 m

Reynold's number is considered one of the flow parameters in the experiment, with different velocities corresponding to the frequencies listed in Table 8, which can be manipulated by changing the flow velocity:

$$\mathrm{Re} = \frac{\rho V y}{\mu} \qquad (8)$$

where ρ is the fluid density, v is the stream velocity, y is the water depth in the water tunnel, and μ is the fluid dynamic viscosity; in this case, the fluid is water.

The stability of the SWS is tested at flow velocities of 0.5 to 1 m/s to produce different Reynold's numbers shown in Table 8. The stability improvement between the previous and the new SWS prototype scale models can be estimated by applying the following equation:

$$\text{Stability Improvement} = \frac{\text{Old distance} - \text{New distance}}{\text{Old distance}} \times 100 \qquad (9)$$

where the old distance represents the change in the wing tip locations of the previous SWS prototype scale model on the X-axis and Y-axis from their initial positions during flight. The New distance refers to the change in the wing tip locations of the new SWS prototype scale model on the X-axis and Y-axis from their initial positions during flight, as shown in Figure 26.

Table 8: Flow parameters changing with respect to the of the frequency during the experiment

Frequency (Hz)	Flow velocity (m/s)	Re (x10^5)
28.3	0.5	3.37
33.9	0.6	4.04
39.6	0.7	4.72
45.2	0.8	5.39
50.9	0.9	6.07
56.5	1	6.74

The experimental procedure for testing the SWS prototype in the water tunnel is meticulously designed to capture comprehensive data on its stability and performance. The setup ensures precise control and detailed observation of the prototype's behavior under varying flow conditions by employing dual cameras and a variable frequency drive. Considering critical parameters such as Reynolds number and flow velocity, alongside Tracker software for video analysis, facilitates a robust evaluation of the SWS's stability improvements. This thorough approach validates the enhancements made in the new prototype design and provides valuable insights for further optimization.

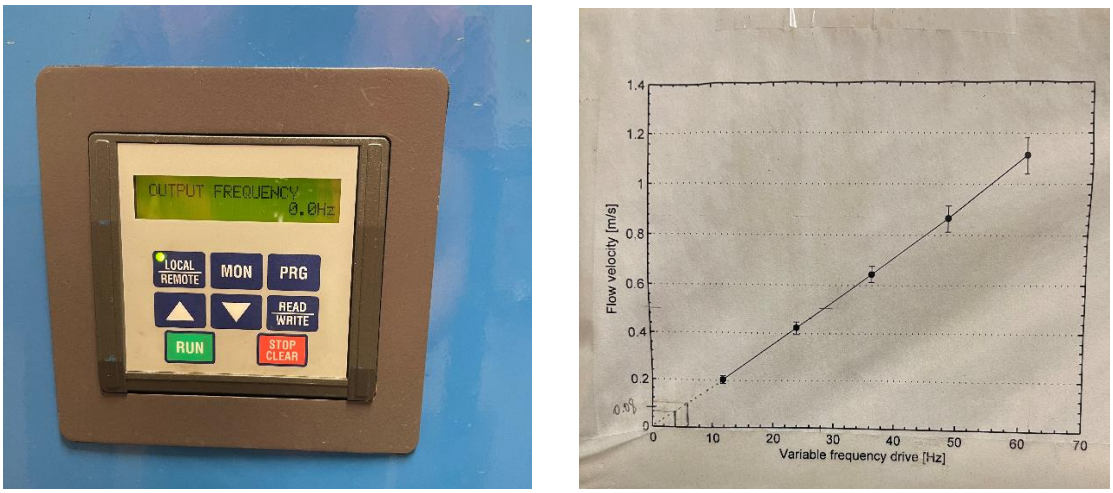

Figure 27: The left side displays the variable-frequency drive, which adjusts the power frequency to modify the flow in the water tunnel. The calibration curve chart on the right illustrates the relationship between flow velocity and variable-frequency drive settings.

4 Results

The SWS is designed and tested for the development of RHKT, with its structure redesigned from a prototype scale model using Xflr5 to assess static and dynamic stability. The first component of the design process allows for the examination of a compatible aerodynamic profile, which is necessary to ensure the stable performance of the turbine. Xflr5 facilitated the determination of the moment, lift, and drag coefficients, as well as the efficiency and functions of the AOA. All four are required for evaluating static stability, with the next step being confirmation of dynamic stability. SolidWorks is used to produce the SWS prototype scale, and the performance of the tail and wing components was tested. This simulation in Xflr5 illustrates how the turbine would appear in three dimensions and how it can function in various circumstances.

The tail and the dihedral angle presented in the design of the SWS provide a significant advantage by maintaining turbine stability in an ever-changing aquatic environment. The tail, a vital design component, significantly improves the SWS's stability. This design ensures that the horizontal stabilizer is positioned at the top of the vertical tail. Hence, it works in relatively undisturbed water, even when the tail is placed 180 degrees in the opposite direction. This separation ensures that the stabilizer effectively maintains the correct direction of flight and stabilizes the body. A sliding mechanism at the top of the vertical piece can be adjusted to keep the AOA for the tail at a positive value when the tail is positioned downward. This feature ensures the SWS remains stable and properly oriented during operation. The design is effective, meaning the SWS structure remains strong and stable throughout its entire operation due to the use of metal screws to secure the segments on a laboratory scale.

The effective stability of the SWS also depends on the dihedral angle of the wing, an aspect captured in the design. A positive dihedral angle, used for polar stability, improves lateral stability. When the wing tips are above the wing roots, the angle enables the SWS to return to its original lateral position, even if disturbed. This aspect is critical for the performance of the SWS in a fluid environment where consistent flow changes can disturb its position. Three dihedral angles, 6°, 10°, and 15°, were investigated in this study to determine which provided the most suitable stability. The results indicated that a positive dihedral angle improves the SWS's ability to maintain its position and withstand rolling motion caused by water currents. Thus, this study's results underscore the effectiveness of the redesigned SWS in enhancing the stability and performance of river RHKT. The innovative design features, such as the tail configuration and adjustable dihedral angles, have significantly improved stability in dynamic aquatic environments. These findings highlight the potential of the SWS design to address the challenges of deploying RHKT in variable river conditions, paving the way for further cost-effective optimization and practical application in remote and cold regions.

4.1 Xflr5 simulation

Following the establishment of the SWS design specifications, testing included static and dynamic stability tests performed in Xflr5 based on a water tunnel environment. Water density was the fluid density with velocity parameters set from 0.5 to 1 m/s. A velocity of 1 m/s matched the highest velocity at which the SWS prototype scale was tested within the water tunnel. The simulation data shows that the SWS is statically stable, as shown in **Error! Reference source not found.** and Figure 29**.**

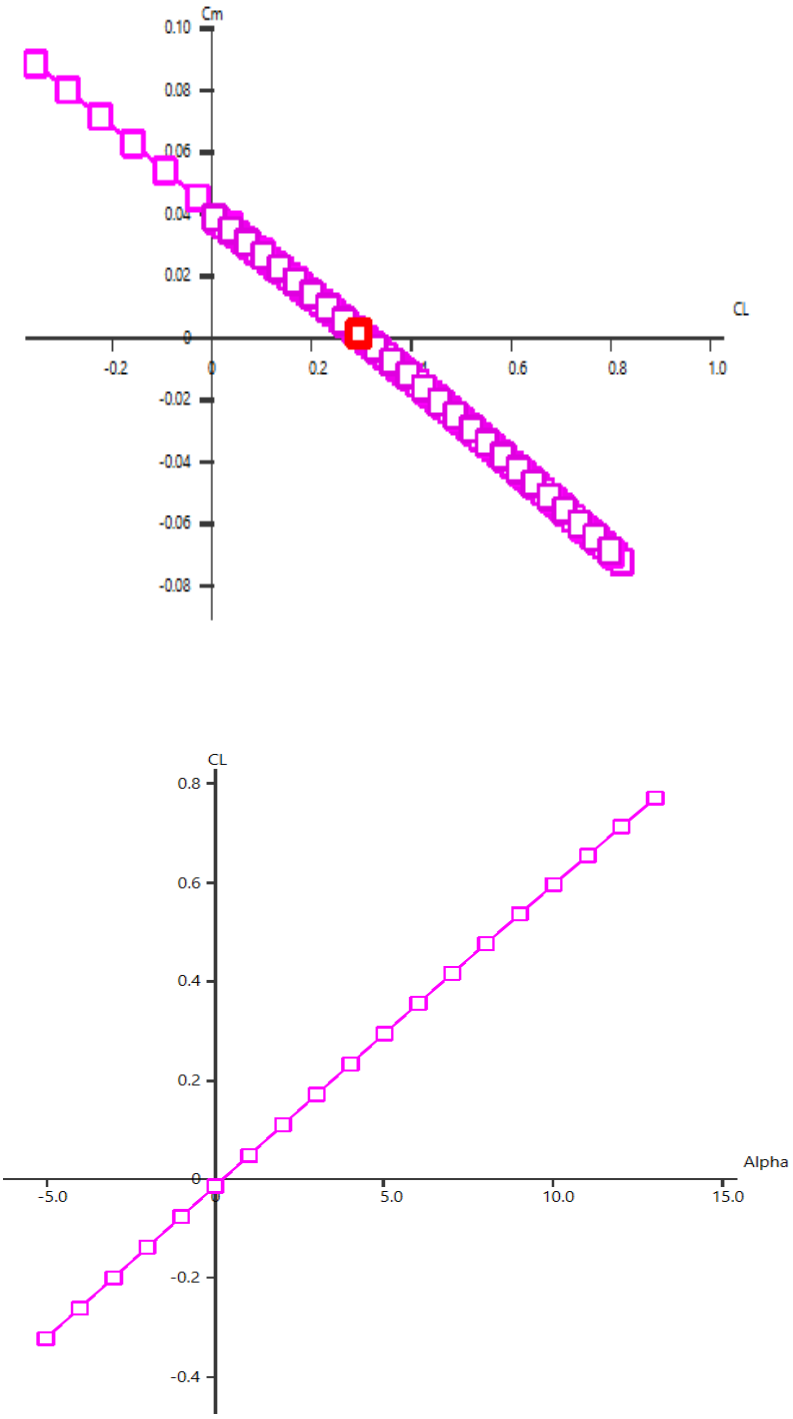

Figure 28: The parameters of static stability were analyzed using Xflr5 software. The upper graph illustrates the plot of the Cm versus the Cl, indicating the stability characteristics of the SWS prototype. A straight line toward a negative value in this plot suggests static stability. The lower graph displays the plot of the Cl versus Alpha, representing the AOA. This graph is essential for understanding how lift varies with changes in AOA.

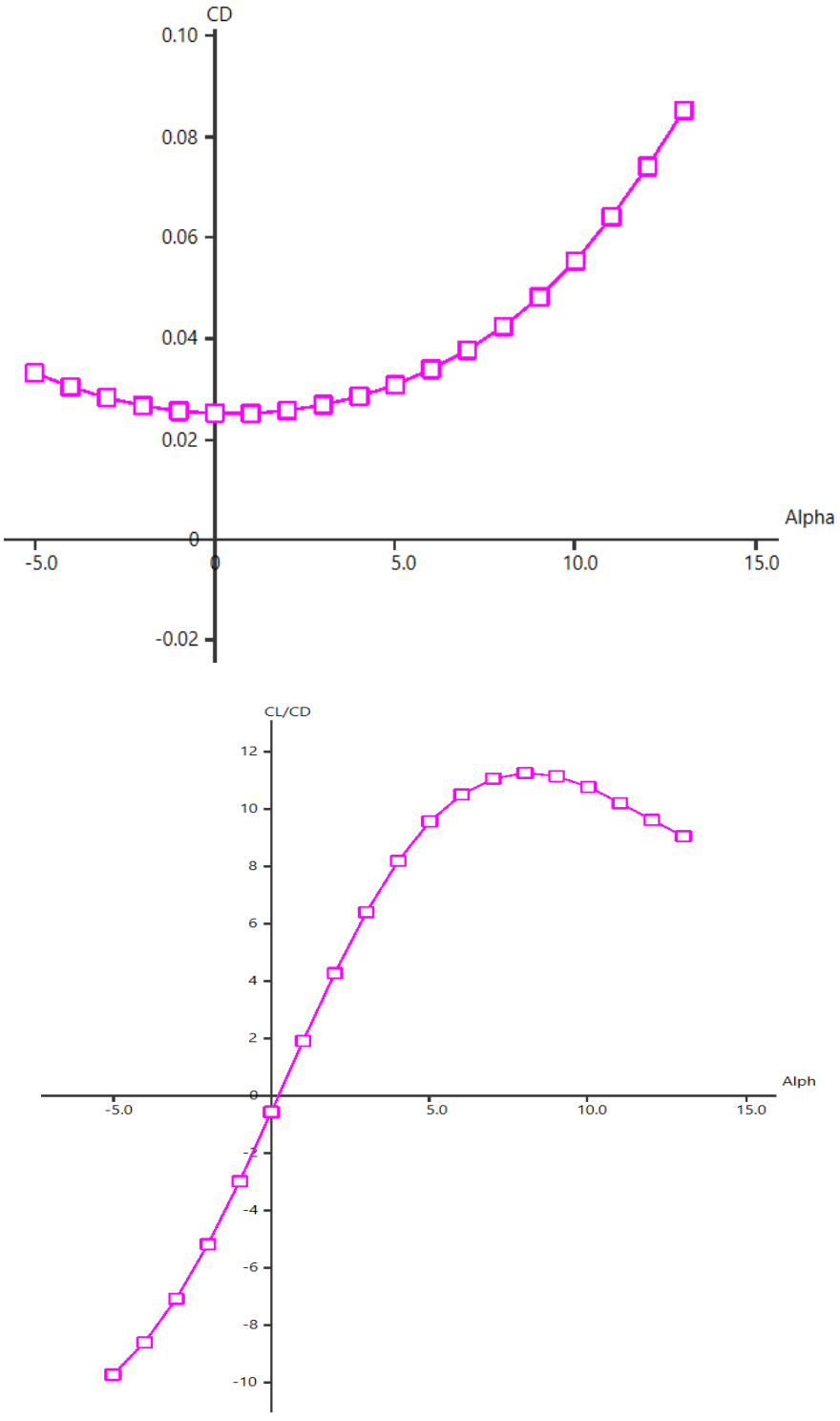

Figure 29: The upper graph presents the plot of the Cd versus the AOA, illustrating that drag increases with an increase in AOA. The lower graph depicts the lift-to-drag ratio Cl/Cd versus AOA, showing a decline in the Cl/Cd ratio beyond an AOA of 8°, indicative of the onset of stall conditions.

The two conditions for static and dynamic stability, which can be seen in the previous figures, include:

1- The Cm vs. C_l plot is a straight line headed toward negative value and

2- The intersection of the C_m vs C_l plot is on the X-axis.

The simulation shows that the SWS design is statically and dynamically stable based on these two conditions. In addition, Figure 30 shows the simulation of the induced and viscous drag change, downwash, surface velocity, Cp, moment, and lift by changing the AOA.

After achieving the first two conditions for static stability to progress to dynamic stability, as mentioned in Section 3, the simulation shows that when the AOA is -5°, the lift force is negative, and the SWS heads downward. Additionally, the Cp value is approximately -1.6 at the leading edge of the airfoil, while along the rest, the Cp is approximately -0.53. However, when the AOA is changed to a positive value, both lift and Cp values are changed, as shown in Figure 30. At an AOA of 8°, the lift changes from negative to positive, with the Cp value at the airfoil's leading edge around 2.7 and the rest at around 0.33. Furthermore, the simulation indicates that the SWS model has achieved natural dynamic stability, which is the tendency of an aircraft to return to its original position after being disturbed [115]. When an external force changes its position, the model returns to its original position after 1-3 seconds. Table 9 below is the dynamic stability information for the SWS simulation used in Xflr5.

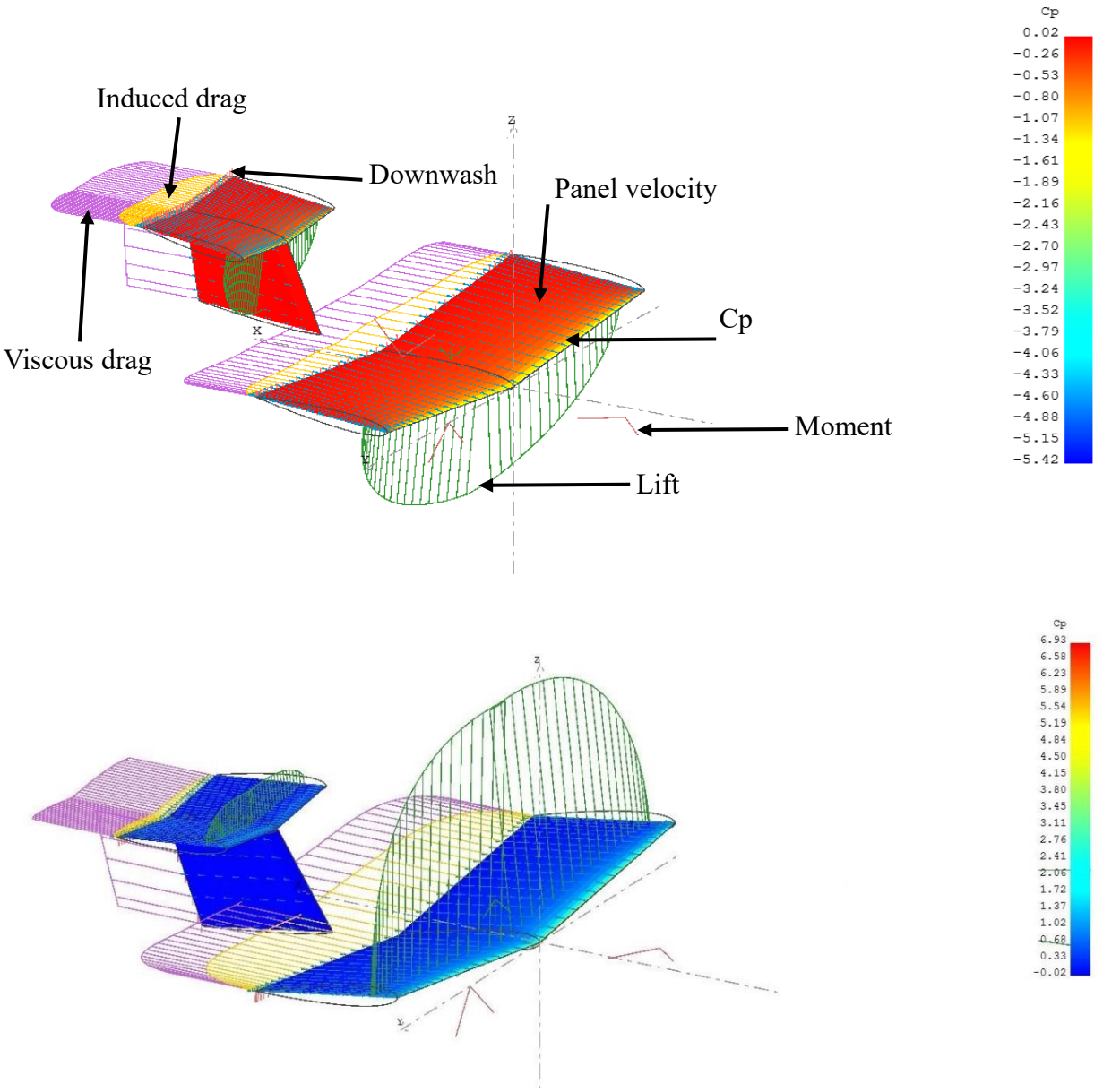

Figure 30**:** The upper illustration depicts the aerodynamic parameters, including induced and viscous drag, downwash, surface velocity, pressure coefficient (Cp), moment, and lift, at an AOA of -5°. The lower illustration contrasts these parameters at an AOA of 8°, highlighting the changes in aerodynamic forces and flow characteristics. The color gradient on the body indicates the Cp value, providing a visual representation of pressure distribution across the surface.

Table 9: Dynamic stability calculated by the Xflr5 software for the simulation type 3-D-Panels/VLM2 as applied to the SWS prototype model (table spans 2 pages)

Best stability performance	Non-dimensional stability derivatives	Non-dimensional control derivatives	Longitudinal modes	Lateral modes
VInf =1.104 m/s AOA = 4.96° Mass = 0.000 g Control value = 1 XNP = 0.049 m XCP = 0.032 m YCP = 0.000 m ZCP = 0.012 m CL = 0.29382 CD = 0.02886 VCD = 0.02090 ICD = 0.00797 CX = 0.00797 CY = -0.00002 Cl = -0.00000 Cm = 0.00150 ICm = 0.00000 VCm = 0.00150 Cn = -0.00002	CXu = -0.04358 CLu = -0.00302 Cmu = -0.00183 CXa = 0.10671 CLa = 3.69423 Cma = -0.49076 CXq = 0.18703 CLq = 5.83917 Cmq = -4.63435 CYb = -0.23667 Clb = -0.07081 Cnb = 0.08691 CYp = -0.05521 Clp = -0.29502 Cnp = -0.06298 CYr = 0.30494 Clr = 0.09859 Cnr = -0.12502	CXd = 0.00 CYd = 0.00 CZd = 0.00 Cld = 0.00 Cmd = 0.00 Cnd = 0.00	Eigenvalue = -112.56842+ 0.0i Undamped Natural Frequency = 0.000 Hz Damped Natural Frequency = 0.000 Hz Damping Ratio = 0.000 Normalized Eigenvector: u/u0 = 0.90552+ 0.00i w/u0 = 31.22709+ 0.00i q/(2.u0.MAC) = -0.38653+ 0.00i theta(rad) = 1.00 + 0.00i Eigenvalue = -10.08133+ 0.00i Undamped Natural Frequency = 0.00 Hz Damped natural frequency = 0.000 Hz Damping Ratio = 0.000 Normalized Eigenvector: u/u0 = 0.90552 + 0.00i w/u0 = 1.01690 + 0.00i q/(2.u0.MAC) = -0.74853+ 0.00i theta(rad) = 1.00 + 0.00i Eigenvalue = -0.78011-1.50185i Undamped Natural Frequency = 0.269 Hz Damped Natural Frequency = 0.239 Hz Damping Ratio = 0.461 Normalized Eigenvector: u/u0 = 0.90552+ 0.00i	Eigenvalue = -162.97147 + 0.00i Undamped Natural Frequency = 0.000 Hz Damped Natural Frequency = 0.000 Hz Damping Ratio = 0.000 Time to double = 0.004s Time constant = 0.006 Normalized Eigenvector: v/u0 = 0.90552 + 0.00i p/(2.u0.Span) = 66.89652 + 0.00i r/(2.u0.Span) = -2.82374 + 0.00i phi(rad) = 1.00 + 0.00i Eigenvalue = -5.55334 + 0.00i Undamped Natural Frequency = 0.000 Hz Damped Natural Frequency = 0.000 Hz Damping Ratio = 0.000 Time to double = 0.125s Time constant = 0.180 Normalized Eigenvector: v/u0 = 0.90552 + 0.00i p/(2.u0.Span) = -0.88850 + 0.00i r/(2.u0.Span) = -1.73204 + 0.00i phi(rad) = 1.00 + 0.00i

ICn = -0.00001 VCn = -0.00000			w/u0 = -0.17176 - 0.00716i q/(2.u0.MAC) = 0.01864 + 0.00336i theta(rad) = 1.00 + 0.00i Eigenvalue = -0.78011+ 1.50185i Undamped Natural Frequency = 0.269 Hz Damped Natural Frequency = 0.239 Hz Damping Ratio = 0.461 Normalized Eigenvector: u/u0 = 0.90552+ 0.00i w/u0 = -0.17176+ 0.00716i q/(2.u0.MAC) = 0.01864 - 0.00336i theta(rad) = 1.00+ 0.00i	Eigenvalue = -5.04065 + 0.00i Undamped Natural Frequency = 0.000 Hz Damped Natural Frequency = 0.000 Hz Damping Ratio = 0.000 Time to double = 0.138s Time constant = 0.198 Normalized Eigenvector: v/u0 = 0.90552 + 0.00i p/(2.u0.Span) = -1.23552 + 0.00000i r/(2.u0.Span) = -2.67303 + 0.00000i phi(rad) = 1.00 + 0.00i Eigenvalue = -0.04290 + 0.00i Undamped Natural Frequency = 0.000 Hz Damped Natural Frequency = 0.000 Hz Damping Ratio = 0.000 Time to double = 16.156s Time constant = 23.308 Normalized Eigenvector: v/u0 = 0.90552 + 0.00i p/(2.u0.Span) = -0.00361+ 0.00i r/(2.u 0.Span) = 0.63910 + 0.00i phi(rad) = 1.00 + 0.00i

The C_l is negative for AOA -5° and -2°, approaching a positive value as the AOA increases towards positive angles. The C_l is negligible at an AOA of 0°; however, it increases to a positive value of 0.103 at an AOA of 2°. The C_m initially has a positive value of 0.089 at an AOA of -5°. As the

AOA increases, the C_m continues to decrease. The C_l value increases progressively at AOA of 5°, 8°, and beyond. However, the C_l/C_d value declines as the AOA value rises to higher levels. The highest coefficient of lift-to-drag ratio (Cl/Cd) is 10.9 at an AOA of 8°, beginning to decline and reaching 10.4 and 8.9 at an AOA of 10° and 13°, respectively. Furthermore, the Cl/Cd ratio continues decreasing as the AOA increases. The C_m value reaches zero at an AOA of 5° and becomes negative as the AOA increases beyond 5°. The Xflr5 simulation shows that the values of C_l and C_d for all three SWS prototype scale models at the AOA range of -5° to 13° are similar, as shown in Table 10, with Figure 31 illustrating these values.

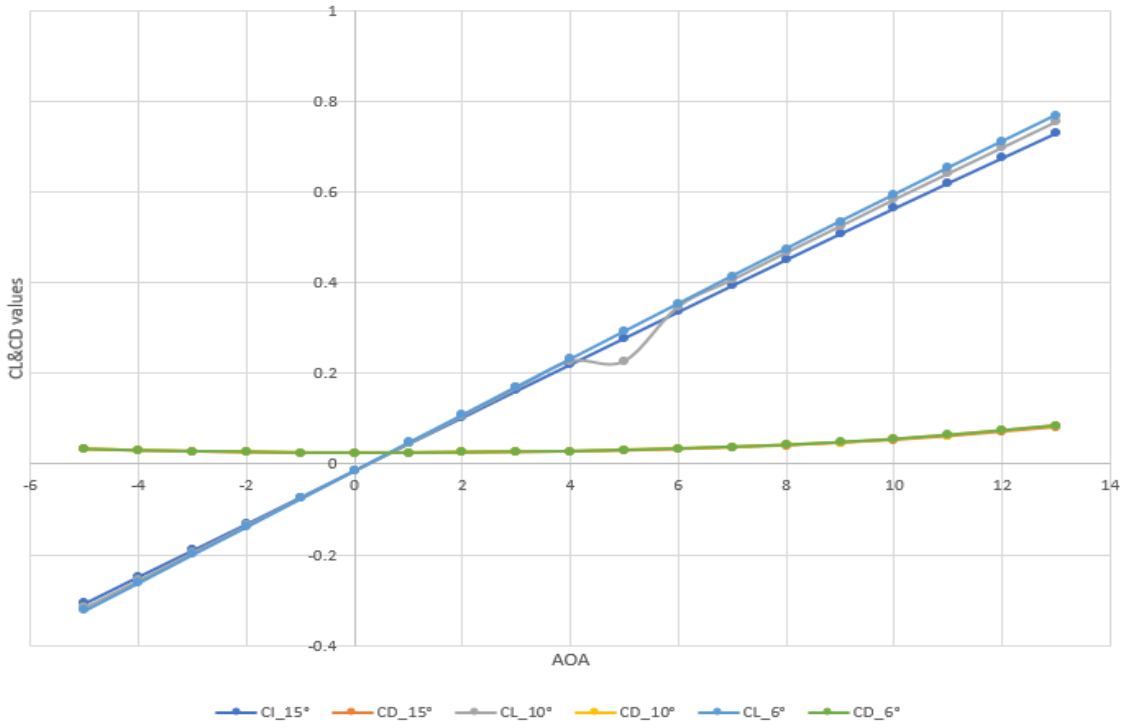

Figure 31: The Cl and Cd plotted against the AOA for three SWS models. The data reveals that the new SWS prototype scale model with a 6° dihedral angle exhibits the most linear behavior among the models tested. This linearity indicates a more predictable and stable aerodynamic performance, crucial for maintaining control and efficiency in varying flow conditions.

Table 10: C_l and C_d values for the 6°, 10°, and 15° dihedral angles SWS models at AOA range from -5° to 13°

AOA	Cl of 6°	Cd of 6°	Cl of 10°	Cd of 10°	Cl of 15°	Cd of 15°
-5	-0.322	0.033	-0.316	0.033	-0.307	0.033
-4	-0.261	0.03	-0.256	0.03	-0.284	0.03
-3	-0.199	0.028	-0.195	0.028	-0.19	0.028
-2	-0.138	0.027	-0.135	0.027	-0.132	0.026
-1	-0.076	0.025	-0.075	0.025	-0.073	0.025
0	-0.014	0.025	-0.014	0.025	-0.014	0.025
1	0.048	0.025	0.046	0.025	0.045	0.025
2	0.109	0.026	0.107	0.026	0.103	0.026
3	0.171	0.027	0.168	0.027	0.162	0.027
4	0.232	0.028	0.228	0.028	0.22	0.028
5	0.293	0.031	0.228	0.031	0.278	0.03
6	0.354	0.034	0.348	0.034	0.336	0.033
7	0.415	0.038	0.407	0.037	0.394	0.037
8	0.475	0.042	0.467	0.042	0.451	0.041
9	0.535	0.048	0.525	0.047	0.508	0.047
10	0.594	0.055	0.584	0.054	0.564	0.053
11	0.653	0.064	0.641	0.063	0.62	0.061
12	0.711	0.074	0.698	0.073	0.675	0.071
13	0.769	0.085	0.755	0.084	0.73	0.081

The longitudinal and lateral stabilities, which maintain the original position for the design during the flight, are improved in this design. These results are expected in the first stage of designing the SWS prototype scale model to enhance its stability. Moreover, the panel force is extracted from the simulation to determine its value when the AOA is negative and positive, as shown in Figure 32, which illustrates the variation of the panel force on the wing and tail for AOA of -5° and 5°, along with the flow pattern behind the SWS prototype. For both AOA, the panel force is maximum at the airfoil's leading edge and decreases rapidly in the first quarter of the airfoil where it becomes negligible. Moreover, the force does not vary along the airfoil itself. For an AOA of -5°, the panel force varies from 5.125 to -1734 Pa and acts downwards; the force varies from -113.44 to 1292.74

Pa and acts upwards for an AOA of 5°. The downward force for negative AOA allows the model to dive into the first step of launching the turbine into the river, as shown in Figure 3, detailing the deployment produced. As the AOA is increased during deployment, the force becomes positive, allowing the SWS turbine to fly within the water column and proceed with deployment. The positive panel force allows the turbine to operate at the target water depth within the water column for a given river velocity by keeping the AOA at a fixed positive value. Recall that the relationship between velocity and AOA is based on the harness wire lengths. For these simulation results shown in Figure 32, the resulting wing load is 18.4 kg/m^2. The panel force for the tail follows the same trend as for the wing, as shown in Figure 32.

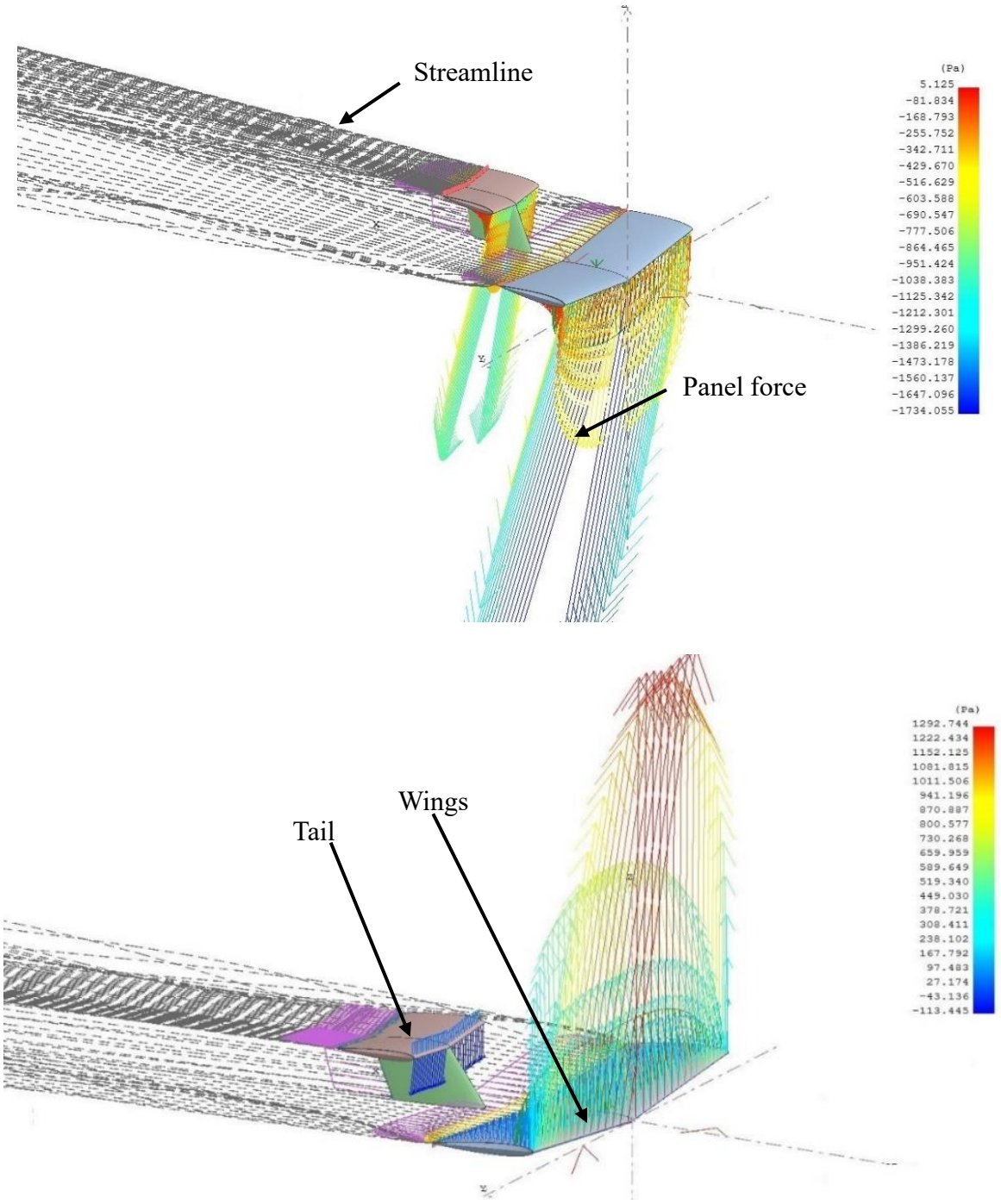

Figure 32: The panel force distribution in Pascals along the airfoils of the wing and tail, accompanied by the downstream streamlines, for the new SWS prototype scale models. The upper illustration represents a negative AOA of- 5 °, while the lower illustration depicts a positive AOA of 5°. The wings' aspect ratio is 3.385, which influences the aerodynamic efficiency and stability of the models.

As a result, the Xflr5 simulation results affirm the hypothesis that the SWS can significantly enhance the stability and performance of RHKT, thereby addressing the LCOE and facilitating market acceptance in cold climates. The simulation demonstrated that the SWS design achieves static and dynamic stability, which is crucial for maintaining operational efficiency in variable aquatic environments. The ability of the SWS to maintain stability through strategic aerodynamic features, such as the adjustment of the AOA and the optimization of lift-to-drag ratios, underscores its potential to simplify deployment and retrieval processes. This capability is particularly beneficial for operating below ice layers, maximizing power generation, and ensuring the system's resilience in cold climates. The findings suggest that while the SWS approach is currently limited to small-scale systems, its design principles could be pivotal in reducing costs and enhancing the viability of RHKT systems in challenging environments.

4.2 Water tunnel testing results

Water tunnel testing results show a significant improvement in the design of the SWS by incorporating tail and dihedral angle wings, which together enhance the system's stability as expected. The old and new SWS prototype scale models were tested in the water tunnel under identical conditions to investigate system stability enhancement. The improvement in SWS stability aligned with the expectations of this research. The figures below illustrate the stability improvement after testing and analyzing the behavior of both models in the water tunnel.

Therefore, the previous SWS prototype scale model in the upper graph in Figure 33 demonstrates low stability and a twist to the right direction at a velocity of 0.6 m/s, ultimately crashing at 0.8 m/s. The previous SWS model exhibits less roll and yaw stability, beginning to angle horizontally as it twists until the lever arm touches the water tunnel wall, leading to a crash. The angle reaches about

60° with the horizontal when it starts to crash into the wall, and the distance between the two wing tip locations is approximately 30 cm. Such a crash can explain critical failures experienced by flying a stainless-steel prototype at the CHTTC during winter 2022. In contrast, the new model, shown in the lower graph, displays high roll and yaw stability with no twisting or crashing, even at a velocity of 1 m/s. The lower graph in Figure 32 also shows a small oscillation at the same level for both wing tips, with the value of these oscillations around 1 cm at flow velocities of 0.5, 0.6, and 0.7 m/s, respectively. However, oscillations increase to around 2.5 cm at a flow velocity of 0.8 m/s before returning to 1 cm at 0.9 m/s. The maximum distance between the two wing tips is about 4 cm, which is minimal compared to the previous SWS model shown in the top graph in Figure 33. Data indicates much higher stability to flow velocity in the water tunnel for the Y-axis of the new SWS.

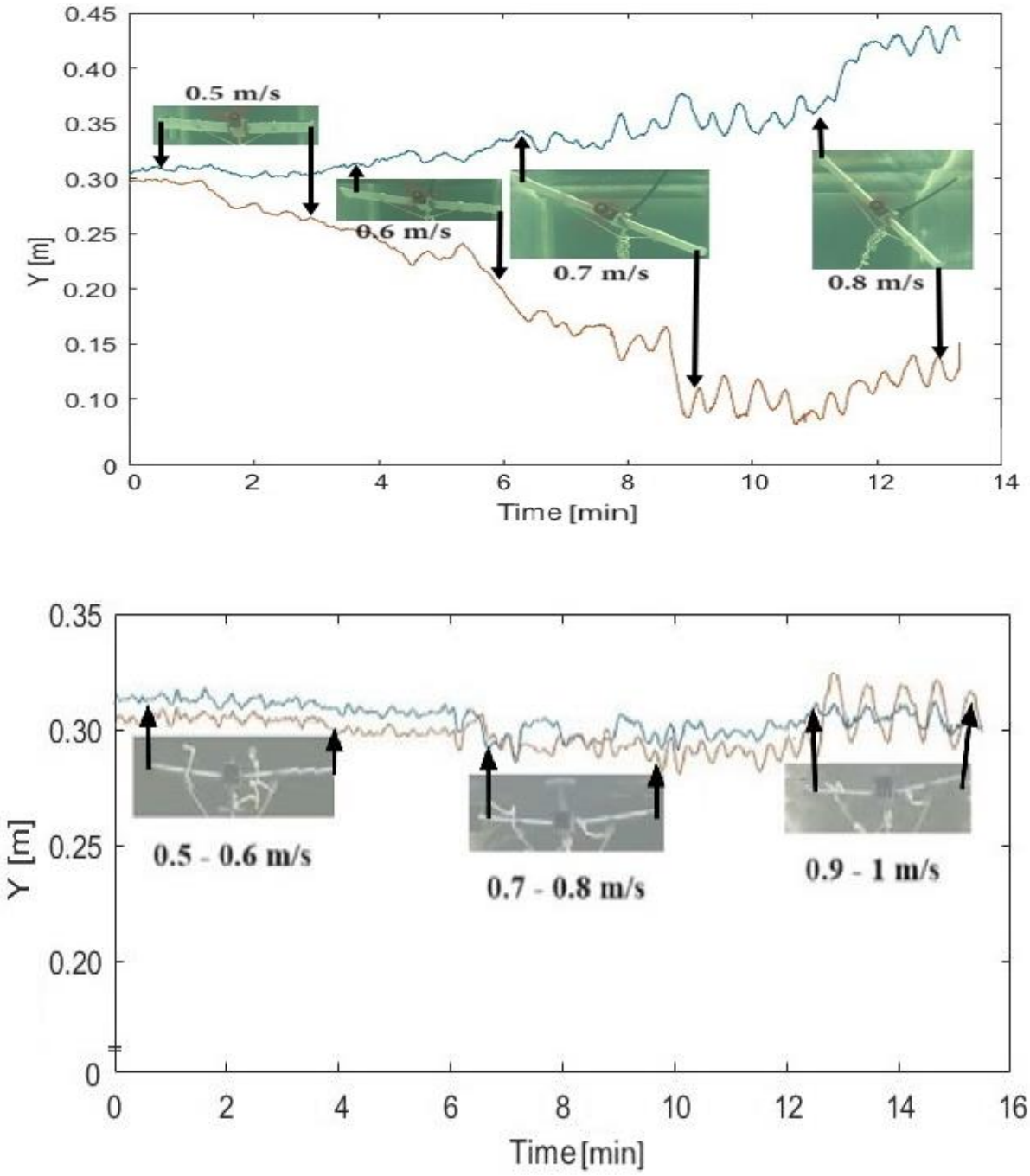

Figure 33: The performance of the previous SWS prototype scale model with the new SWS prototype scale model featuring a 6° dihedral angle. In both graphs, the red line indicates the left-wing tip, while the blue line represents the right-wing tip. The upper graph illustrates the variation in wing tip locations on the Y-axis at different velocities for the previous SWS model, highlighting its instability and tendency to twist at higher velocities. The lower graph shows the corresponding changes for the new SWS model, demonstrating improved stability and reduced oscillations, even at increased flow velocities.

The previous SWS prototype scale model, as shown in the upper graph in Figure 34, exhibits low stability and begins to twist at a flow velocity of 0.6 m/s, eventually crashing into the right-side wall of the water tunnel at 0.8 m/s. Additionally, the previous SWS model experiences a few oscillations during operation but lacks control over roll and yaw stability due to the absence of a tail and a dihedral angle for the wings. In contrast, the new SWS prototype scale model, shown in the lower graph in Figure 34, demonstrates high stability with small oscillations on the X-axis, avoiding crashes even at a velocity of 1 m/s. These oscillations are regular movements in such an environment, starting at around 2 cm at 0.5 and 0.6 m/s velocities. The oscillations increase to a maximum of 5 cm on the X-axis at velocities of 0.7, 0.8, and 0.9 m/s, respectively, but decrease to 3 cm when the flow velocity reaches 1 m/s. This behavior indicates that the design has high roll and yaw stability at different velocities in the water tunnel.

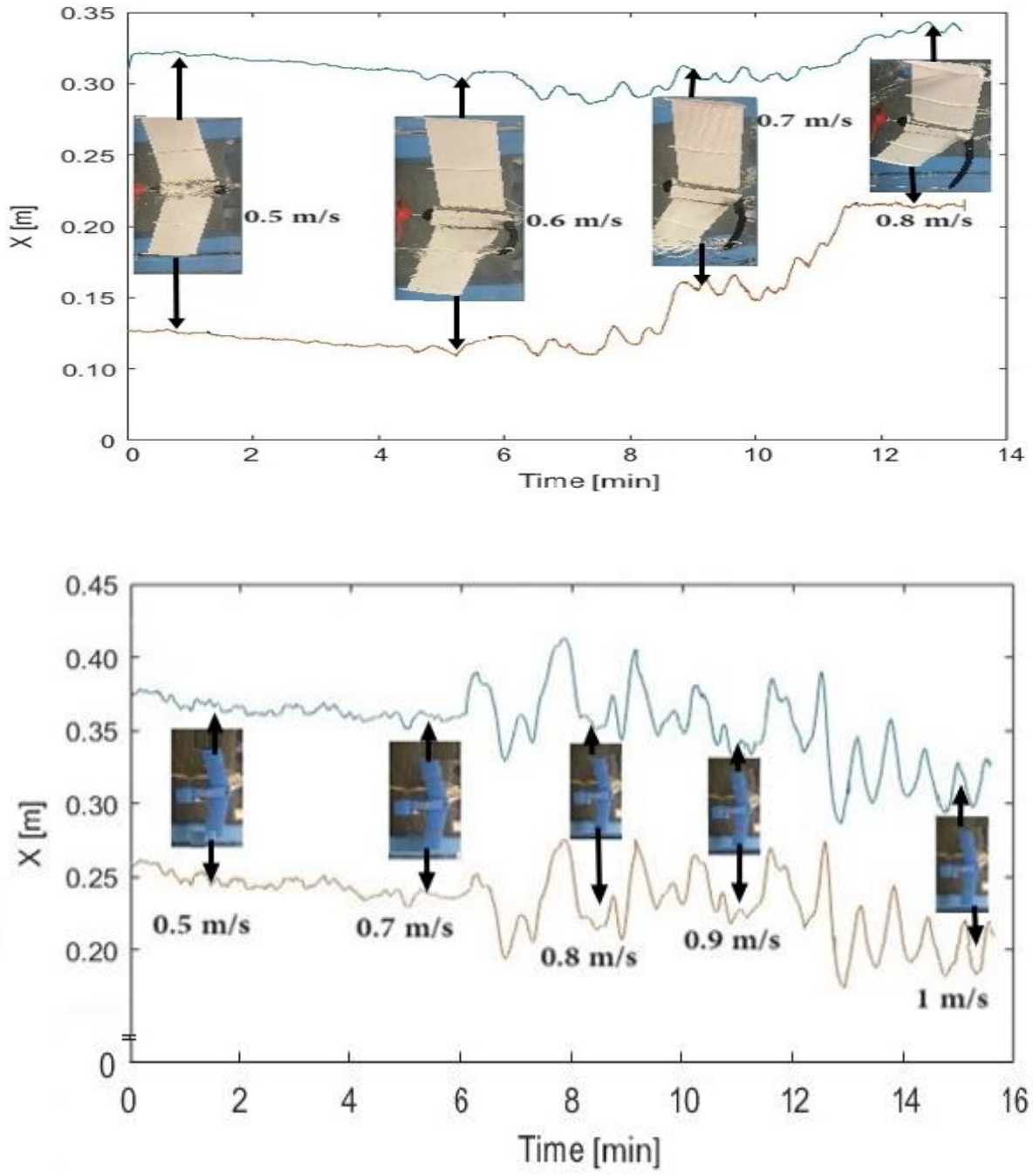

Figure 34: The performance of the previous SWS prototype scale model with the new SWS prototype scale model featuring a 6° dihedral angle. The red line indicates the tip of the left wing, while the blue line represents the tip of the right wing. The upper graph illustrates the changes in wing tip locations on the X-axis at various velocities for the previous SWS model. It highlights its instability and tendency to twist, leading to crashes at higher velocities. The lower graph shows the corresponding changes for the new SWS model, demonstrating enhanced stability and reduced oscillations, even at increased flow velocities, due to the improved design with a dihedral angle.

The figure below shows the new SWS prototype scale model with 10° and 15° dihedral angles, and both SWS models show acceptable stability at a velocity of 0.7 m/s on both the Y-axis and X-axis, with small oscillations on both axes. These figures also reveal a small gap between the wing tips for both models on the Y-axis, which presents an issue in the stability of the systems. However, the models can still be considered stable due to their constant performance, as shown in Figure 35.

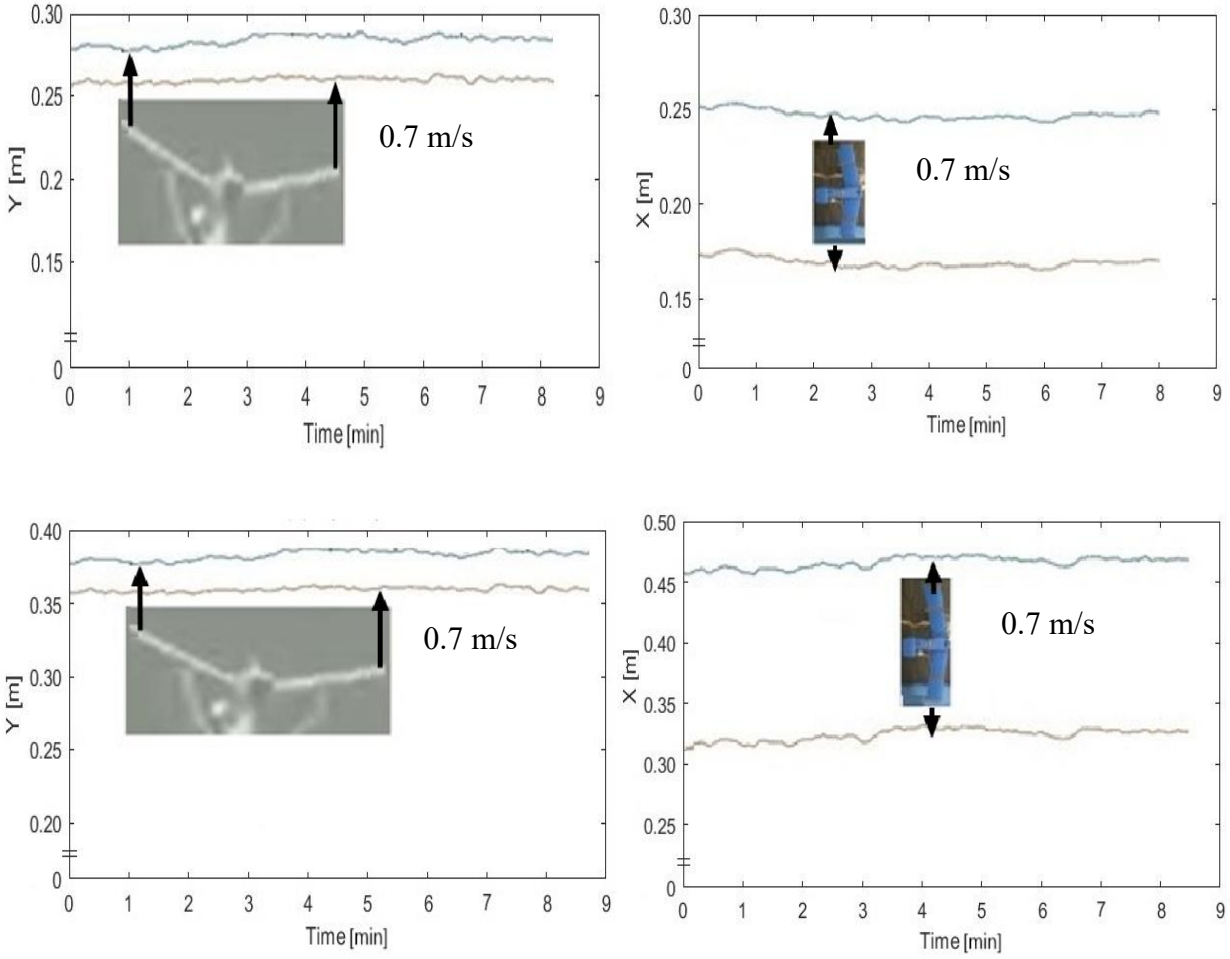

Figure 35: The performance of the new SWS models with 10° and 15° dihedral angles. The two upper graphs represent the performance of the SWS model with a 10° dihedral angle, showing the wing tip locations on the Y-axis and X-axis at a velocity of 0.7 m/s. The two lower graphs depict the performance of the SWS model with a 15° dihedral angle under the same velocity conditions. Both models demonstrate acceptable stability with minor oscillations on both axes. However, a small gap between the wing tips on the Y-axis is observed, which could affect stability. Despite this, the models maintain consistent performance, indicating their overall stability.

The stability decreases for both 10° and 15° dihedral angle SWS prototype scale models at a flow velocity of 9 m/s, as shown in Figure 36. The SWS model with the 10° dihedral angle still exhibits acceptable stability at this velocity. Although it has a gap of about 5 cm between the wing tips on the Y-axis, it can be considered stable due to its constant performance, as shown in the figure.

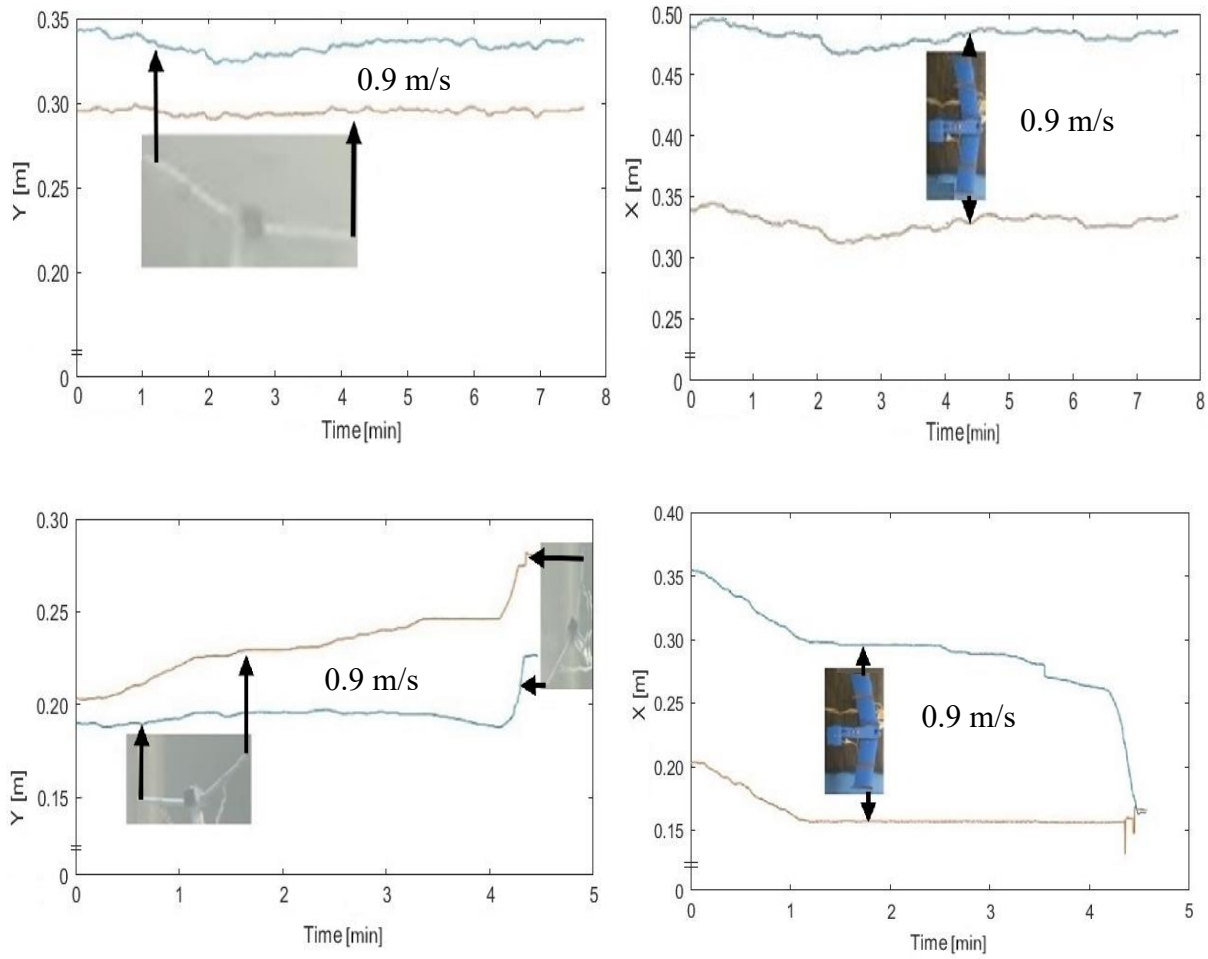

Figure 36: The performance of SWS models with 10° and 15° dihedral angles at a flow velocity of 0.9 m/s. The upper graphs show the 10° model's stable performance with consistent wing tip gaps and minor oscillations. The lower graphs reveal the 15° model's increasing instability, with widening wing tip gaps and twisting, leading to a crash. These results suggest a maximum safe operating velocity of 0.7 m/s for the 15° model.

In Figure 36, the SWS model with 10° shows that there is a distance between the wing tips of about 5 cm on the Y-axis at a flow velocity of 0.9 m/s, and this distance compounds with small oscillations but remains constant with respect to time, as shown above. Also, it shows a small oscillation with continuous distance on the X-axis in Figure 36, but it also remains constant with respect to time, which can result in stability in the model with a 10° dihedral angle. On the other hand, a 15° dihedral angle SWS performance on the Y-axis in Figure 36The figure shows the distance between the wing tips starting at 2 cm and continuing to increase until it crashes into the water tunnel wall. Figure 36 shows the SWS performance beginning at 15 cm on the X-axis, which becomes smaller with time, resulting from the twisting angle of the SWS until it crashes into the water tunnel wall. So, it exhibits the same behavior as the previous SWS model, but the difference is that the 15° dihedral angle SWS model crashes at a flow velocity of 0.9 m/s. In this case, the 15° dihedral angle SWS model cannot survive at a flow velocity of more than 0.8 m/s, and to be on the safe side, the flow velocity must be a maximum of 0.7 m/s for the 15° dihedral angle SWS model on a water tunnel scale. The result of the SWS, tail up and tail down, was similar in terms of stability.

The increase in the dihedral angle can create issues with the design stability, and the increase in the flow turbulence and the flow velocity increase causes damping issues for the SWS, which impacts its stability. According to the testing results, the 6° dihedral angle SWS model is more stable than the 10° and 15° dihedral angle SWS models. The 15° dihedral angle SWS model is the least stable among the three dihedral angle models. However, the following results can be documented by comparing new SWS model testing results with the previous SWS model testing results and considering the flow tolerance increase as the flow velocity increases.

- The 6° dihedral angle SWS model stability is improved by around 80% to 90% for flow velocities of 0.5, 0.6, and 0.7 m/s, respectively, and 75 to 80% for flow velocities of 0.8, 0.9, and 1 m/s, respectively. This is a significant improvement in stability, and it could apply to the tidal HKT systems, reducing their cost, especially removing the turbine for maintenance.
- The 10° dihedral angle SWS model stability is improved by around 50% to 60% for flow velocities of 0.5 and 0.6 m/s, respectively, and 45% to 50% for flow velocities of 0.7, 0.8, 0.9, and 1 m/s, respectively.
- The 15° dihedral angle SWS model stability is improved by around 40% to 50% for flow velocities 0.5 and 0.6 m/s, respectively, and 25% to 30% for flow velocities 0.7, 0.8, 0.9, and 1 m/s, respectively.

The water tunnel testing results underscore the potential of the SWS to address the high LCOE and facilitate the market acceptance of RHKT systems in cold climates. The SWS design has significantly improved stability by incorporating tail and dihedral angle wings, particularly at lower flow velocities. The enhanced stability of the 6° dihedral angle SWS model, which outperforms the 10° and 15° models, highlights the importance of optimizing design parameters to achieve operational efficiency. These findings suggest that the SWS can effectively simplify deployment and retrieval processes, operate efficiently below ice layers, and maintain resilience in cold environments. Although currently limited to small-scale systems, the SWS design principles offer a promising pathway to reduce costs and improve the viability of RHKT systems in challenging conditions.

5 Conclusions

The study investigated the effect of using the SWS for RHKT systems by focusing on enhancing power generation in cold weather regions. The results showed that the design and development of the SWS tested using Xflr5 simulation software and water tunnel experiments demonstrated significant improvements in static and dynamic stability over the prototype. Among the 6°, 10°, and 15° dihedral angles tested with the new SWS model, the optimal dihedral angle of 6° was identified as providing the highest stability (more than 80%), which is crucial for the reliable operation of RHKT systems in varying environmental conditions. Thus, the SWS can address several logical problems associated with RHKT systems. It reduces the high LCOE by simplifying deployment, retrieval, and maintenance processes and lowering costs, especially in cold climates. The SWS's ability to surface and submerge allows it to avoid ice formation and debris, mitigating mechanical failures and operational issues. By operating within the water column, the SWS minimizes interference with riverine activities and environmental disruption, promoting sustainable deployment. Dihedral-angle wings and a tail design enhance stability and efficiency across varying flow velocities and turbulence levels, ensuring consistent power generation.

Furthermore, the SWS's multifunctional components and advanced design strategies support scalability and adaptability, making it effective in diverse river conditions. The study also discussed the economic and logistic challenges of deploying RHKT, including ice formation, turbine mounting, and performance enhancement. The innovative design of the SWS, with its ability to surface and submerge the turbine, offers a practical solution to these challenges, potentially reducing costs and improving the efficiency of hydrokinetic energy generation. The ability of the SWS to surface and submerge the turbine as needed provides a practical solution to

the issues posed by ice layers, allowing for continuous operation even in harsh conditions. The SWS is designed to operate efficiently below the ice in the water column, maximizing power generation potential. By maintaining stability and control in varying environmental conditions, the SWS ensures that the turbine can harness the kinetic energy of river currents effectively. Incorporating tail and dihedral angle wings, particularly the optimal 6° dihedral angle, enhances the static and dynamic stability of the system. The design of the SWS emphasizes the multifunctionality of its components, ensuring that each element contributes to the deployment, retrieval, and operational phases. This approach reduces the system's complexity and minimizes the need for additional equipment, lowering overall costs. The use of advanced simulation software and water tunnel testing has demonstrated the effectiveness of this design strategy.

However, the study faced limitations due to the control of the flow velocities and the limited size of the water tunnel, which limited the tested model size. Thus, tested flow velocities (0.5 to 1 m/s) may not represent natural river conditions. This indicates that further research is necessary to enhance performance across diverse flow conditions. Although the SWS shows significant promise, it is restricted to relatively small-scale systems. This limitation is primarily due to the need for further testing and validation in more energetic river environments. Future research should focus on scaling up the SWS design and evaluating its performance in diverse conditions to fully realize its potential in reducing the LCOE of RHKT systems. Additionally, exploring the integration of the SWS with existing hydrokinetic technologies could provide valuable insights into its applicability and effectiveness in larger-scale applications.

Recommendations to improve the SWS system includes

1. Test the larger-scale SWS in an energetic river environment and evaluate the system stability.
2. Test the new SWS models considering the power cable and the torque resulting from the generator and the rotor.
3. Investigate why the new SWS model with a 6° dihedral angle has greater stability than the SWS with 10° and 15° dihedral angles.
4. Characterize the power curve for the scaled and new larger-scale SWS turbine.
5. Combine the new SWS with a smart control system to better control the operation and gain the advantage of remote control of surfacing and submerging the new SWS.
6. Enhance the new SWS material selection to offer better durability and resistance to harsh environmental conditions, such as ice formation and debris impact.
7. Conduct economic analyses to assess the cost-effectiveness of the SWS in comparison to other renewable energy solutions. This includes evaluating the lifecycle of costs, potential savings, and return on investment for remote and off-grid communities.

References

[1] R. McMaster, B. Noble, and G. Poelzer, "Assessing local capacity for community appropriate sustainable energy transitions in northern and remote Indigenous communities," *Renew. Sustain. Energy Rev.*, vol. 191, p. 114232, Mar. 2024, doi: 10.1016/j.rser.2023.114232.

[2] Canada Energy Regulator, "Canada energy regulator market snapshot overcoming the challenges of powering Canada's off-grid communities," 2018. Accessed: Jun. 06, 2024. [Online]. Available: https://www.cer-rec.gc.ca/en/data-analysis/energy-markets/market-snapshots/2018/market-snapshot-overcoming-challenges-powering-canadas-off-grid-communities.html

[3] V. Menghwani, R. Wheat, B. Balicki, G. Poelzer, B. Noble, and N. Mansuy, "Bioenergy for community energy security in Canada: Challenges in the business ecosystem," *Energies*, vol. 16, no. 4, p. 1560, Feb. 2023, doi: 10.3390/en16041560.

[4] R. J. Hewitt *et al.*, "Social innovation in community energy in Europe: A review of the evidence," *Front. Energy Res.*, vol. 7, p. 31, Apr. 2019, doi: 10.3389/fenrg.2019.00031.

[5] D. Newell, A. Sandström, and P. Söderholm, "Network management and renewable energy development: An analytical framework with empirical illustrations," *Energy Res. Soc. Sci.*, vol. 23, pp. 199–210, Jan. 2017, doi: 10.1016/j.erss.2016.09.005.

[6] M. J. Pasqualetti, T. E. Jones, L. Necefer, C. A. Scott, and B. J. Colombi, "A paradox of plenty: Renewable energy on Navajo nation lands," *Soc. Nat. Resour.*, vol. 29, no. 8, pp. 885–899, Aug. 2016, doi: 10.1080/08941920.2015.1107794.

[7] J. P. Brewer Ii, S. Vandever, and J. T. Johnson, “Towards energy sovereignty: Biomass as sustainability in interior Alaska,” *Sustain. Sci.*, vol. 13, no. 2, pp. 417–429, Mar. 2018, doi: 10.1007/s11625-017-0441-5.

[8] G. Holdmann, D. Pride, G. Poelzer, B. Noble, and C. Walker, “Critical pathways to renewable energy transitions in remote Alaska communities: A comparative analysis,” *Energy Res. Soc. Sci.*, vol. 91, p. 102712, Sep. 2022, doi: 10.1016/j.erss.2022.102712.

[9] K. Jenkins, B. K. Sovacool, and D. McCauley, “Humanizing sociotechnical transitions through energy justice: An ethical framework for global transformative change,” *Energy Policy*, vol. 117, pp. 66–74, Jun. 2018, doi: 10.1016/j.enpol.2018.02.036.

[10] C. Walker, G. Poelzer, R. Leonhardt, B. Noble, and C. Hoicka, “COPs and ‘robbers’: Better understanding community energy and toward a Communities of Place then Interest approach,” *Energy Res. Soc. Sci.*, vol. 92, p. 102797, Oct. 2022, doi: 10.1016/j.erss.2022.102797.

[11] F. W. Geels, “Technological transitions as evolutionary reconfiguration processes: A multi-level perspective and a case-study,” *Res. Policy*, vol. 31, no. 8–9, pp. 1257–1274, Dec. 2002, doi: 10.1016/S0048-7333(02)00062-8.

[12] C. A. Miller, J. O’Leary, E. Graffy, E. B. Stechel, and G. Dirks, “Narrative futures and the governance of energy transitions,” *Futures*, vol. 70, pp. 65–74, Jun. 2015, doi: 10.1016/j.futures.2014.12.001.

[13] N. Smith, L. Baugh Littlejohns, and D. Thompson, “Shaking out the cobwebs: Insights into community capacity and its relation to health outcomes,” *Community Dev. J.*, vol. 36, no. 1, pp. 30–41, Jan. 2001, doi: 10.1093/cdj/36.1.30.

[14] J. M. Bauer and P. M. Herder, “Designing socio-technical systems,” in *Philosophy of Technology and Engineering Sciences*, Elsevier, 2009, pp. 601–630. doi: 10.1016/B978-0-444-51667-1.50026-4.

[15] R. Bullock, D. Kirchhoff, I. Mauro, and M. Boerchers, “Indigenous capacity for collaboration in Canada’s energy, forestry and mining sectors: Research metrics and trends,” *Environ. Dev. Sustain.*, vol. 20, no. 2, pp. 883–895, Apr. 2018, doi: 10.1007/s10668-017-9917-9.

[16] J. I. Schmidt, B. Johnson, H. P. Huntington, and E. Whitney, “A framework for assessing food-energy-water security: A FEW case studies from rural Alaska,” *Sci. Total Environ.*, vol. 821, p. 153355, May 2022, doi: 10.1016/j.scitotenv.2022.153355.

[17] C. E. Hoicka, K. Savic, and A. Campney, “Reconciliation through renewable energy: A survey of Indigenous communities, involvement, and peoples in Canada,” *Energy Res. Soc. Sci.*, vol. 74, p. 101897, Apr. 2021, doi: 10.1016/j.erss.2020.101897.

[18] F. Avelino and J. M. Wittmayer, “Shifting power relations in sustainability transitions: A multi-actor perspective,” *J. Environ. Policy Plan.*, vol. 18, no. 5, pp. 628–649, Oct. 2016, doi: 10.1080/1523908X.2015.1112259.

[19] M. R. Quitoras, P. E. Campana, P. Rowley, and C. Crawford, “Remote community integrated energy system optimization including building enclosure improvements and quantitative energy trilemma metrics,” *Appl. Energy*, vol. 267, p. 115017, Jun. 2020, doi: 10.1016/j.apenergy.2020.115017.

[20] R. Leonhardt, B. Noble, G. Poelzer, P. Fitzpatrick, K. Belcher, and G. Holdmann, “Advancing local energy transitions: A global review of government instruments supporting

community energy," *Energy Res. Soc. Sci.*, vol. 83, p. 102350, Jan. 2022, doi: 10.1016/j.erss.2021.102350.

[21] C. J. R. Walker, M. B. Doucette, S. Rotz, D. Lewis, H. T. Neufeld, and H. Castleden, "Non-Indigenous partner perspectives on Indigenous peoples' involvement in renewable energy: Exploring reconciliation as relationships of accountability or status quo innocence?," *Qual. Res. Organ. Manag. Int. J.*, vol. 16, no. 3/4, pp. 636–657, Nov. 2021, doi: 10.1108/QROM-04-2020-1916.

[22] M. Kamal, G. Saini, A. Abbas, and V. Prasad, "Prediction and analysis of the cavitating performance of a Francis turbine under different loads," *Energy Sources Part Recovery Util. Environ. Eff.*, pp. 1–25, Nov. 2021, doi: 10.1080/15567036.2021.2009941.

[23] M. S. Güney and K. Kaygusuz, "Hydrokinetic energy conversion systems," *Renew. Sustain. Energy Rev.*, vol. 14, no. 9, pp. 2996–3004, Dec. 2010, doi: 10.1016/j.rser.2010.06.016.

[24] P. P. Gohil and R. P. Saini, "Coalesced effect of cavitation and silt erosion in hydro turbines," *Renew. Sustain. Energy Rev.*, vol. 33, pp. 280–289, May 2014, doi: 10.1016/j.rser.2014.01.075.

[25] C. S. Kaunda, C. Z. Kimambo, and T. K. Nielsen, "Hydropower in the context of sustainable energy supply: A review of technologies and challenges," *ISRN Renew. Energy*, vol. 2012, pp. 1–15, Dec. 2012, doi: 10.5402/2012/730631.

[26] O. Doso and S. Gao, "An overview of small hydro power development in India," *AIMS Energy*, vol. 8, no. 5, pp. 896–917, 2020, doi: 10.3934/energy.2020.5.896.

[27] C. P. Jawahar and P. A. Michael, "A review on turbines for micro hydro power plant," *Renew. Sustain. Energy Rev.*, vol. 72, pp. 882–887, May 2017, doi: 10.1016/j.rser.2017.01.133.

[28] W. Rehman, F. Rehman, and M. Z. Malik, “A review of Darrieus water turbines,” in *Volume 2: Heat Exchanger Technologies; Plant Performance; Thermal Hydraulics and Computational Fluid Dynamics; Water Management for Power Systems; Student Competition*, Lake Buena Vista, Florida, USA: American Society of Mechanical Engineers, Jun. 2018, p. V002T12A015. doi: 10.1115/POWER2018-7547.

[29] M. Rakibuzzaman, S.-H. Suh, H.-H. Kim, Y. Ryu, and K. Y. Kim, “Development of a hydropower turbine using seawater from a fish farm,” *Processes*, vol. 9, no. 2, p. 266, Jan. 2021, doi: 10.3390/pr9020266.

[30] K. Kusakana and H. J. Vermaak, “Hydrokinetic power generation for rural electricity supply: Case of South Africa,” *Renew. Energy*, vol. 55, pp. 467–473, Jul. 2013, doi: 10.1016/j.renene.2012.12.051.

[31] K. Kusakana, “Feasibility analysis of river off-grid hydrokinetic systems with pumped hydro storage in rural applications,” *Energy Convers. Manag.*, vol. 96, pp. 352–362, May 2015, doi: 10.1016/j.enconman.2015.02.089.

[32] Md. M. Kamal and R. P. Saini, “A review on modifications and performance assessment techniques in cross-flow hydrokinetic system,” *Sustain. Energy Technol. Assess.*, vol. 51, p. 101933, Jun. 2022, doi: 10.1016/j.seta.2021.101933.

[33] M. J. Khan, G. Bhuyan, M. T. Iqbal, and J. E. Quaicoe, “Hydrokinetic energy conversion systems and assessment of horizontal and vertical axis turbines for river and tidal applications: A technology status review,” *Appl. Energy*, vol. 86, no. 10, pp. 1823–1835, Oct. 2009, doi: 10.1016/j.apenergy.2009.02.017.

[34] E. Lalander and M. Leijon, “In-stream energy converters in a river – effects on upstream hydropower station,” *Renew. Energy*, vol. 36, no. 1, pp. 399–404, Jan. 2011, doi: 10.1016/j.renene.2010.05.019.

[35] A. H. Birjandi, J. Woods, and E. L. Bibeau, “Investigation of macro-turbulent flow structures interaction with a vertical hydrokinetic river turbine,” *Renew. Energy*, vol. 48, pp. 183–192, Dec. 2012, doi: 10.1016/j.renene.2012.04.045.

[36] K. Kusakana, “Techno-economic analysis of off-grid hydrokinetic-based hybrid energy systems for onshore/remote area in South Africa,” *Energy*, vol. 68, pp. 947–957, Apr. 2014, doi: 10.1016/j.energy.2014.01.100.

[37] V. B. Miller, E. W. Ramde, R. T. Gradoville, and L. A. Schaefer, “Hydrokinetic power for energy access in rural Ghana,” *Renew. Energy*, vol. 36, no. 2, pp. 671–675, Feb. 2011, doi: 10.1016/j.renene.2010.08.014.

[38] Armin Hamta, “A remotely operated hydrokinetic turbine to reduce the levelized cost of energy of marine turbines,” Master’s thesis, University of Manitoba, Manitoba, Canada, 2016.

[39] D. L. Talavera, E. Muñoz-Cerón, J. De La Casa, D. Lozano-Arjona, M. Theristis, and P. J. Pérez-Higueras, “Complete procedure for the economic, financial and cost-competitiveness of photovoltaic systems with self-consumption,” *Energies*, vol. 12, no. 3, p. 345, Jan. 2019, doi: 10.3390/en12030345.

[40] Thake, J, “Development, installation and testing of a large-scale tidal current turbine,” IT Power (United Kingdom); Marine Current Turbines (United Kingdom); Seacore (United Kingdom); Bendalls Engineering (United Kingdom); Corus (United Kingdom), United Kingdom, Technical Report T-06/00210/00/REP; URN-05/1698, Oct. 2005.

[41] B. Kirke, “Towards more cost-effective river hydrokinetic turbines,” *Energy Sustain. Dev.*, vol. 78, p. 101370, Feb. 2024, doi: 10.1016/j.esd.2023.101370.

[42] S. Bahador, “Using numerical analysis to design and optimize river hydrokinetic turbine to address seasonal velocity variations,” Master’s Thesis, University of Manitoba, Canada, 2023. [Online]. Available: http://hdl.handle.net/1993/37193

[43] E. Bibeau *et al.*, “Design of in-situ river kinetic turbines test facility in cold water,” *Proc. Can. Eng. Educ. Assoc. CEEA*, Aug. 2011, doi: 10.24908/pceea.v0i0.3775.

[44] Bibeau, Eric, Shamez Kassam, J. Woods, Tom Molinski, and Clayton Bear, “Operating a 5-kW grid-connected hydro kinetic turbine in a river in cold climates,” *Can. J. Ocean Eng.*, vol. 35, pp. 67–79, 2009.

[45] F. Taveira-Pinto, P. Rosa-Santos, and T. Fazeres-Ferradosa, “Marine renewable energy,” *Renew. Energy*, vol. 150, pp. 1160–1164, May 2020, doi: 10.1016/j.renene.2019.10.014.

[46] F. Taveira-Pinto, G. Iglesias, P. Rosa-Santos, and Z. D. Deng, “Preface to special topic: Marine renewable energy,” *J. Renew. Sustain. Energy*, vol. 7, no. 6, p. 061601, Nov. 2015, doi: 10.1063/1.4939086.

[47] D. M. Fouz, R. Carballo, V. Ramos, and G. Iglesias, “Hydrokinetic energy exploitation under combined river and tidal flow,” *Renew. Energy*, vol. 143, pp. 558–568, Dec. 2019, doi: 10.1016/j.renene.2019.05.035.

[48] M. Musa, C. Hill, and M. Guala, “Interaction between hydrokinetic turbine wakes and sediment dynamics: Array performance and geomorphic effects under different siting strategies and sediment transport conditions,” *Renew. Energy*, vol. 138, pp. 738–753, Aug. 2019, doi: 10.1016/j.renene.2019.02.009.

[49] E. E. Lust, K. A. Flack, and L. Luznik, "Survey of the near wake of an axial-flow hydrokinetic turbine in the presence of waves," *Renew. Energy*, vol. 146, pp. 2199–2209, Feb. 2020, doi: 10.1016/j.renene.2019.08.067.

[50] V. Stratigaki, P. Troch, and D. Forehand, "A fundamental coupling methodology for modeling near-field and far-field wave effects of floating structures and wave energy devices," *Renew. Energy*, vol. 143, pp. 1608–1627, Dec. 2019, doi: 10.1016/j.renene.2019.05.046.

[51] Woodruff A, "An economic assessment of renewable energy options for rural electrification in Pacific Island countries," *Pac. Isl. Appl. Geosci. Comm. SOPAC*, p. 96, 2007.

[52] C. Boccaletti, G. Fabbri, J. Marco, and E. Santini, "An overview on renewable energy technologies for developing countries: The case of Guinea Bissau," *Renew. Energy Power Qual. J.*, vol. 1, no. 06, pp. 343–348, Mar. 2008, doi: 10.24084/repqj06.295.

[53] O. Paish, "Small hydro power: Technology and current status," *Renew. Sustain. Energy Rev.*, vol. 6, no. 6, pp. 537–556, Dec. 2002, doi: 10.1016/S1364-0321(02)00006-0.

[54] H. J. Vermaak, K. Kusakana, and S. P. Koko, "Status of micro-hydrokinetic river technology in rural applications: A review of literature," *Renew. Sustain. Energy Rev.*, vol. 29, pp. 625–633, Jan. 2014, doi: 10.1016/j.rser.2013.08.066.

[55] T. Hoq, U.A. Nawshad, N. Islam, K. Syfullah, and R. Rahman, "Micro hydro power: Promising solution for off-grid renewable energy source," *Int. J. Sci. Eng. Res.*, vol. 2, 2011.

[56] J. Sowers, A. Vengosh, and E. Weinthal, "Climate change, water resources, and the politics of adaptation in the Middle East and North Africa," *Clim. Change*, vol. 104, no. 3–4, pp. 599–627, Feb. 2011, doi: 10.1007/s10584-010-9835-4.

[57] D. C. Maniaci and Y. Li, “Investigating the influence of the added mass effect to marine hydrokinetic horizontal-axis turbines using a general dynamic wake wind turbine code,” *Mar. Technol. Soc. J.*, vol. 46, no. 4, pp. 71–78, Jul. 2012, doi: 10.4031/MTSJ.46.4.4.

[58] P. Mycek, B. Gaurier, G. Germain, G. Pinon, and E. Rivoalen, “Numerical and experimental study of the interaction between two marine current turbines,” *Int. J. Mar. Energy*, vol. 1, pp. 70–83, Apr. 2013, doi: 10.1016/j.ijome.2013.05.007.

[59] M.A. Arango, “Resource assessment and feasibility study for use of hydrokinetic turbines in the tailwaters of the Priest Rapids project,” Master’s Thesis, University of Washington, USA, 2011.

[60] A. Ruopp, A. Ruprecht, S. Riedelbauch, G. Arnaud, and I. Hamad, “Development of a hydro kinetic river turbine with simulation and operational measurement results in comparison,” *IOP Conf. Ser. Earth Environ. Sci.*, vol. 22, no. 6, p. 062002, Mar. 2014, doi: 10.1088/1755-1315/22/6/062002.

[61] M. Ridgill, S. P. Neill, M. J. Lewis, P. E. Robins, and S. D. Patil, “Global riverine theoretical hydrokinetic resource assessment,” *Renew. Energy*, vol. 174, pp. 654–665, Aug. 2021, doi: 10.1016/j.renene.2021.04.109.

[62] G. Miller, J. Franceschi, W. Lese, J. Rico, “The allocation of kinetic hydro energy conversion systems (KHECS) in USA drainage basins: Regional resource and potential power,” Final Report, 1986.

[63] UMA Group, “An evaluation of the kinetic energy of Canadian rivers & Estuaries,” Tech. Rep, 1980.

[64] Environment Canada, “National water data archive: HYDAT,” 2018. [Online]. Available: https://www.canada.ca/en/environment-climate-change/ services/water-overview/quantity/monitoring/survey/data-products-services/national-archive-hydat.html

[65] M. Kummu, H. De Moel, P. J. Ward, and O. Varis, “How close do we live to water? A global analysis of population distance to freshwater bodies,” *PLoS ONE*, vol. 6, no. 6, p. e20578, Jun. 2011, doi: 10.1371/journal.pone.0020578.

[66] M. J. Khan, M. T. Iqbal, and J. E. Quaicoe, “River current energy conversion systems: Progress, prospects, and challenges,” *Renew. Sustain. Energy Rev.*, vol. 12, no. 8, pp. 2177–2193, Oct. 2008, doi: 10.1016/j.rser.2007.04.016.

[67] J. Riglin, W. C. Schleicher, and A. Oztekin, “Diffuser optimization for a micro-hydrokinetic turbine,” in *Volume 7: Fluids Engineering Systems and Technologies*, Montreal, Quebec, Canada: American Society of Mechanical Engineers, Nov. 2014, p. V007T09A077. doi: 10.1115/IMECE2014-37304.

[68] A. Q. Al-Shetwi, “Sustainable development of renewable energy integrated power sector,” *Sci. Total Environ.*, vol. 822, p. 153645, May 2022, doi: 10.1016/j.scitotenv.2022.153645.

[69] D. Scott and S. Gössling, “Destination net-zero: What does the international energy agency roadmap mean for tourism?,” *J. Sustain. Tour.*, vol. 30, no. 1, pp. 14–31, Jan. 2022, doi: 10.1080/09669582.2021.1962890.

[70] N. R. Maldar, C. Y. Ng, and E. Oguz, “A review of the optimization studies for Savonius turbine considering hydrokinetic applications,” *Energy Convers. Manag.*, vol. 226, p. 113495, Dec. 2020, doi: 10.1016/j.enconman.2020.113495.

[71] R. E. H. Sims, H.-H. Rogner, and K. Gregory, “Carbon emission and mitigation cost comparisons between fossil fuel, nuclear and renewable energy resources for electricity

generation," *Energy Policy*, vol. 31, no. 13, pp. 1315–1326, Oct. 2003, doi: 10.1016/S0301-4215(02)00192-1.

[72] M. Mulligan, A. Van Soesbergen, and L. Sáenz, "Goodd, a global dataset of more than 38,000 georeferenced dams," *Sci. Data*, vol. 7, no. 1, p. 31, Jan. 2020, doi: 10.1038/s41597-020-0362-5.

[73] "TECHNOLOGY ROADMAP," in *SpringerReference*, Berlin/Heidelberg: Springer-Verlag, 2011. doi: 10.1007/SpringerReference_7300.

[74] F. Behrouzi, M. Nakisa, A. Maimun, and Y. M. Ahmed, "Global renewable energy and its potential in Malaysia," *Renew. Sustain. Energy Rev.*, vol. 62, pp. 1270–1281, Sep. 2016, doi: 10.1016/j.rser.2016.05.020.

[75] Z. Ma, R. Jiang, D. Wang, and K. Zhang, "Fault mode, effects and criticality analysis for overheating fault of wind turbines gearbox and generator," in *International Conference on Renewable Power Generation (RPG 2015)*, Beijing, China: Institution of Engineering and Technology, 2015, p. 5 .-5 . doi: 10.1049/cp.2015.0445.

[76] L. G. Scherer and R. F. De Camargo, "Control of micro hydro power stations using nonlinear model of hydraulic turbine applied on microgrid systems," in *XI Brazilian Power Electronics Conference*, Natal, Brazil: IEEE, Sep. 2011, pp. 812–818. doi: 10.1109/COBEP.2011.6085260.

[77] A. J. Fleming, "Aquantis ocean current turbine development project report," DOE/EE0002648, 1150234, Aug. 2014. doi: 10.2172/1150234.

[78] S. Oh, "Evaluation of four rugged long-term velocity measurement methods for assessment of hydrokinetic energy production," Master's Thesis, University of Manitoba, Manitoba, Canada, 2023.

[79] M. Shahsavarifard, A. H. Birjandi, E. L. Bibeau, and R. Sinclaire, "Performance characteristics of the energy cat 3EC42 hydrokinetic turbine," in *OCEANS 2015 - Genova*, Genova, Italy: IEEE, May 2015, pp. 1–4. doi: 10.1109/OCEANS-Genova.2015.7271420.

[80] Amir Garanovic, "Second RivGen reaches Alaska," *OFFSHOR ENERGY*, Aug. 09, 2021.

[81] J. Thomson, L. Kilcher, and B. Polagye, "RivGen current flow measurements, Igiugig, AK." Marine and Hydrokinetic Data Repository (MHKDR); Ocean Renewable Power Company, p. 1, 2014. doi: 10.15473/1418350.

[82] K. W. Tan, B. Kirke, and M. Anyi, "Small-scale hydrokinetic turbines for remote community electrification," *Energy Sustain. Dev.*, vol. 63, pp. 41–50, Aug. 2021, doi: 10.1016/j.esd.2021.05.005.

[83] S. d'Auteuil, "Investigation of velocity and turbulence measurement techniques for riverine hydrokinetic turbine sites," Master's Thesis, University of Manitoba, Manitoba, Canada, 2016.

[84] S. Kassam, "In-situ testing of a Darrieus hydrokinetic turbine in cold climates," Master's Thesis, University of Manitoba, Manitoba, Canada, 2009.

[85] J. Woods, "Hydrokinetic turbine Systems for remote river applications in cold climates," University of Manitoba, Manitoba, Canada, 2017.

[86] A. H. Birjandi, S. d'Auteuil, C. Ridd, and E. L. Bibeau, "An innovative low cost hydrokinetic site selection technique for cold climate regions," in *OCEANS 2015 - Genova*, Genova, Italy: IEEE, May 2015, pp. 1–4. doi: 10.1109/OCEANS-Genova.2015.7271660.

[87] B. Wang, Z. J. Lu, X. B. Chen, P. Wang, W. Luo, and H. Xu, "Modeling and analysis of the dynamic efficiency of manual transmission/reducer," *Int. J. Automot. Technol.*, vol. 16, no. 3, pp. 417–426, Jun. 2015, doi: 10.1007/s12239-015-0043-0.

[88] A. Dolgushin, D. Voronin, and O. Mamonov, “Optimization of resource consumption when using vehicle transmissions at low temperatures,” *J. Eng. Appl. Sci.*, vol. 15, no. 1, pp. 74–80, Oct. 2019, doi: 10.36478/jeasci.2020.74.80.

[89] S. Kulkarni, C. Chapman, H. Shah, E. A. Parn, and D. J. Edwards, “Designing an efficient tidal turbine blade through bio-mimicry: A systematic review,” *J. Eng. Des. Technol.*, vol. 16, no. 1, pp. 101–124, Feb. 2018, doi: 10.1108/JEDT-08-2017-0077.

[90] K. Fischer, F. Besnard, and L. Bertling, “Reliability centered maintenance for wind turbines based on statistical analysis and practical experience,” *IEEE Trans. Energy Convers.*, vol. 27, no. 1, pp. 184–195, Mar. 2012, doi: 10.1109/TEC.2011.2176129.

[91] L. Mahrt, J. Sun, and D. Stauffer, “Dependence of turbulent velocities on wind speed and stratification,” *Bound.-Layer Meteorol.*, vol. 155, no. 1, pp. 55–71, Apr. 2015, doi: 10.1007/s10546-014-9992-5.

[92] Alaska Power and Telephone, “In Alaska tidal energy conference,” Eagle hydrokinetic turbine projec, Alaska, 2007.

[93] S. Kassam, “In-situ testing of a Darrieus hydro kinetic turbine in cold climates,” Master’s Thesis, University of Manitoba, Winnipeg, 2009.

[94] M. Sood and S. K. Singal, “Development of hydrokinetic energy technology: A review,” *Int. J. Energy Res.*, vol. 43, no. 11, pp. 5552–5571, Sep. 2019, doi: 10.1002/er.4529.

[95] L. C. Eme, J. A. Ulasi, A. I. Alade Tunde, and A. C. Odunze, “Hydrokinetic turbines for power generation in Nigerian river basins,” *Water Pract. Technol.*, vol. 14, no. 1, pp. 71–80, Mar. 2019, doi: 10.2166/wpt.2019.001.

[96] C.M. Puertas-Frías, S.C. Willson, and P.A. García-Salaberri, “Design and economic analysis of a hydrokinetic turbine for household applications,” *Renew. Energy*, vol. 199, pp. 587–598, Nov. 2022, doi: 10.1016/j.renene.2022.08.155.

[97] P. Karalekas, G. J. Kowalski, and E. Lovelace, “Modeling Hydrokinetic Turbine Performance in the Mississippi River,” *Mar. Technol. Soc. J.*, vol. 47, no. 4, pp. 57–66, Jul. 2013, doi: 10.4031/MTSJ.47.4.21.

[98] V. S. Neary, B. Gunawan, and D. C. Sale, “Turbulent inflow characteristics for hydrokinetic energy conversion in rivers,” *Renew. Sustain. Energy Rev.*, vol. 26, pp. 437–445, Oct. 2013, doi: 10.1016/j.rser.2013.05.033.

[99] F. Naziano, M. Edileuza, A. Elisa, and M. Johnnn, *Preliminary Analysis of Potential for River Hydrokinetic Energy Technologies in the Amazon River*. https://publications.iadb.org/handle/11319/7292, 2015. doi: 10.18235/0000222.

[100] C. Josias Da Silva and B, Claudio José Cavalcante, “Flow-velocity model for hydrokinetic energy availability assessment in the Amazon,” *Acta Sci. Technol.*, vol. 42, p. e45703, Nov. 2019, doi: 10.4025/actascitechnol.v42i1.45703.

[101] C. M. Niebuhr, M. Van Dijk, V. S. Neary, and J. N. Bhagwan, “A review of hydrokinetic turbines and enhancement techniques for canal installations: Technology, applicability and potential,” *Renew. Sustain. Energy Rev.*, vol. 113, p. 109240, Oct. 2019, doi: 10.1016/j.rser.2019.06.047.

[102] T.T. Muluken, G,D. Dawit, A.T. Bimrew, “Economics of hydrokinetic turbine for off-grid application: A case study of Gumara River, Upper Blue Nile, Amhara, Ethiopia,” *Int. J. Renew. Energy Res.*, no. v9i3, 2019, doi: 10.20508/ijrer.v9i3.9590.g7753.

[103] B. Diego, A. Gonzalo, and C. Lenin, “Design and hydrodynamic analysis of horizontal-axis hydrokinetic turbines with three different hydrofoils by CFD,” *J. Appl. Eng. Sci.*, vol. 18, no. 4, pp. 529–536, 2020, doi: 10.5937/jaes0-25273.

[104] P. K. Modali, A. Vinod, and A. Banerjee, “Towards a better understanding of yawed turbine wake for efficient wake steering in tidal arrays,” *Renew. Energy*, vol. 177, pp. 482–494, Nov. 2021, doi: 10.1016/j.renene.2021.05.152.

[105] K. Golecha, T. I. Eldho, and S. V. Prabhu, “Influence of the deflector plate on the performance of modified Savonius water turbine,” *Appl. Energy*, vol. 88, no. 9, pp. 3207–3217, Sep. 2011, doi: 10.1016/j.apenergy.2011.03.025.

[106] G. Kailash, T. I. Eldho, and S. V. Prabhu, “Performance study of modified Savonius water turbine with two deflector plates,” *Int. J. Rotating Mach.*, vol. 2012, pp. 1–12, 2012, doi: 10.1155/2012/679247.

[107] M.W. Batten, F. Weichbrodt, G.U. Muller, J. Hadler, C. Semlow, M. Hochbaum, S. Dimke, and P. Frohle, “Design and stability of a floating free stream energy converter.,” pp. 2372–2379, Jun. 2011.

[108] D. L. F. Gaden and E. L. Bibeau, “A numerical investigation into the effect of diffusers on the performance of hydro kinetic turbines using a validated momentum source turbine model,” *Renew. Energy*, vol. 35, no. 6, pp. 1152–1158, Jun. 2010, doi: 10.1016/j.renene.2009.11.023.

[109] A. H. Birjandi, E. L. Bibeau, V. Chatoorgoon, and A. Kumar, “Power measurement of hydrokinetic turbines with free-surface and blockage effect,” *Ocean Eng.*, vol. 69, pp. 9–17, Sep. 2013, doi: 10.1016/j.oceaneng.2013.05.023.

[110] D. Magagna and A. Uihlein, “Ocean energy development in Europe: Current status and future perspectives,” *Int. J. Mar. Energy*, vol. 11, pp. 84–104, Sep. 2015, doi: 10.1016/j.ijome.2015.05.001.

[111] S. S. Khalid, Z. Liang, and N. Shah, “Harnessing tidal energy using vertical axis tidal turbine,” *Res. J. Appl. Sci. Eng. Technol.*, vol. 5, no. 1, pp. 239–252, Jan. 2013, doi: 10.19026/rjaset.5.5112.

[112] D. Forbush, R. J. Cavagnaro, J. Donegan, J. McEntee, and B. Polagye, “Multi-mode evaluation of power-maximizing cross-flow turbine controllers,” *Int. J. Mar. Energy*, vol. 20, pp. 80–96, Dec. 2017, doi: 10.1016/j.ijome.2017.09.001.

[113] L. Song, H. Yang, Y. Zhang, H. Zhang, and J. Huang, “Dihedral influence on lateral–directional dynamic stability on large aspect ratio tailless flying wing aircraft,” *Chin. J. Aeronaut.*, vol. 27, no. 5, pp. 1149–1155, Oct. 2014, doi: 10.1016/j.cja.2014.08.003.

[114] R. C. Cheung, D. Rezgui, J. E. Cooper, and T. Wilson, “Analyzing the dynamic behavior of a high aspect ratio wing incorporating a folding wingtip,” Orlando, FL: American Institute of Aeronautics and Astronautics, Jan. 2020. doi: 10.2514/6.2020-2290.

[115] T. T. Takahashi, J. A. Griffin, and R. V. Grandhi, “A review of high-speed aircraft stability and control challenges,” in *AIAA AVIATION 2023 Forum*, San Diego, CA and Online: American Institute of Aeronautics and Astronautics, Jun. 2023. doi: 10.2514/6.2023-3231.